ACOUSTICS EMISSIONS EFFECTS ON RELIABILITY OF SEMICONDUCTORS IN POWER ELECTRONIC DEVICES AND THEIR RELATIONSHIP WITH HEAT GENERATED BY THE DEVICES

A THESIS SUBMITTED TO
THE BOARD OF GRADUATE PROGRAMS
OF
MIDDLE EAST TECHNICAL UNIVERSITY, NORTHERN CYPRUS CAMPUS

BY

MIKE ARASA RATEMO

IN PARTIAL FULFILLMENT OF THE REQUIREMENTS
FOR
THE
DEGREE OF MASTER OF SCIENCE
IN
THE
SUSTAINABLE ENVIRONMENT AND ENERGY SYSTEMS

SEPTEMBER, 2020

Approval of the Board of Graduate Programs

Prof. Dr. Gürkan Karakaş
Chairperson

I certify that this thesis satisfies all the requirements as a thesis for the degree of Master of Science

Asst. Prof. Dr. Ceren Ince
Program Coordinator

This is to certify that we have read this thesis and that in our opinion it is fully adequate, in scope and quality, as a thesis for the degree of Master of Science.

Asst. Prof. Dr. Canras Batunlu
Supervisor

Examining Committee Members

Asst Prof Dr Canras Batunlu	Electrical and Electronics Engineering, METU NCC	______________________
Assoc Prof Dr Murat Fahriglu	Electrical and Electronics Engineering, METU NCC	______________________
Asst Prof Dr Mehmet Şenol	Energy Sys. Engineering CIU	______________________

I hereby declare that all information in this thesis was obtained and presented in accordance with academic rules and ethical conduct. I also declare that, as required by these rules and conduct, I have fully cited and referenced all material and results that are not original to this work.

Name: Mike Arasa Ratemo

Signature :

ABSTRACT

ACOUSTICS EMISSIONS EFFECTS ON RELIABILITY OF SEMICONDUCTORS IN POWER ELECTRONIC DEVICES AND THEIR RELATIONSHIP WITH HEAT GENERATED BY THE DEVICES.

Ratemo, Mike Arasa
MSc Sustainable Environment and Energy Systems
Supervisor: Asst. Prof. Dr Canras Batunlu

September 2020, 73 pages

Power electronics are critical components for energy conversion at all rates. Some of the vital components found in power conversion systems are the switching components, e.g. Insulated Gate Bipolar Transistors (IGBTs). Generally, power switches undergo various failure types that are categorized as packaging problems, e.g., wire bond liftoff. Condition tracking will alleviate the situation substantially by allowing operators to plan converters ' preventive services. Currently, however, there is no consensus on a widely recognized early warning system for errors. In a variety of applications, acoustic emission is typically used as a condition monitoring tool, the best-known being possibly bearing failure detection and rotational machine control. Acoustic signals in the power modules are low, and significant damping is induced by the plastic parts of the power modules. As of now, in power semiconductor modules, acoustic emission is a relatively unknown phenomenon, and there is limited research on the subject. Also, in the previous literature, the focus was mainly on the switching-or failure-related acoustic emissions in power semiconductor modules, most research is focused on the failure associated with the heat generated by the devices. Therefore, the thesis work with the help of COMSOL Multiphysics, we developed a relationship between the heat generated by the IGBTs and the associated acoustic emission to determine their effect on the Reliability of the IGBTs. This enabled us to assess lifetime using the existing lifetime models that factor in the temperature by converting the acoustic emission recorded to a corresponding temperature.

Keywords: Electrothermal Model, IGBT, Acoustics Model, Reliability, Heat

ÖZ

AKUSTİK EMİSYONLARI GÜÇ ELEKTRONİK CİHAZLARDA YARI İLETKENLERİN GÜVENİLİRLİĞİNE VE CİHAZLAR TARAFINDAN ÜRETİLEN ISI İLE İLİŞKİLERİNE ETKİSİ.

Ratemo, Mike Arasa
Yüksek Lisans, Sürdürülebilir Çevre ve Enerji Sistemleri Program
Tez Yöneticisi: Dr. Ögr. Üyesi. Canras Batunlu

Eylül 2020, 73 sayfa

Güç elektroniği, her enerji dönüşümü sistemi için kritik bir bileşendir. Güç dönüştürme sistemlerinde bulunan hayati bileşenlerden bazıları, Yalıtılmış Geçit Bipolar Transistörler (IGBT'ler) gibi anahtarlama cihazlarıdır. Genel olarak, güç anahtarları, paketleme sorunları olarak kategorize edilebilecek çeşitli arıza türlerine maruz kalır (örneğin, bağ kaldırma ve lehim eklemi çatlama hatası). Durum izleme, operatörlerin dönüştürücülerin önleyici hizmetlerini planlamasına izin vererek durumu önemli ölçüde hafifletebilir. Ancak günümüzde, bozulmalar için yaygın olarak tanınan bir erken uyarı sistemi yoktur. Çeşitli uygulamalarda, akustik emisyon bir durum izleme aracı olarak kullanılmıştır, en iyi bilineni arıza algılama ve makine kontrolüdür. Güç modüllerindeki akustik sinyaller düşüktür ve güç modüllerinin plastik kısımları tarafından önemli bir sönümleme indüklenir. Şu an itibariyle, güç yarı iletken modüllerinde akustik emisyon nispeten bilinmeyen bir fenomendir ve konu ile ilgili sınırlı araştırma vardır. Ayrıca, önceki literatürde, güç yarı iletken modüllerindeki anahtarlama veya arızayla ilgili akustik emisyonlardan çok az bahsedilmiş olup, çoğu araştırmada cihazlar tarafından üretilen ısı ile ilişkili arızaya odaklanmıştır.Bu nedenle, tez çalışması COMSOL çoklu fizik yardımıyla, IGBT'lerin ürettiği ısı ile ilgili akustik emisyon arasında IGBT'lerin Güvenilirliği üzerindeki etkisini belirlemek için bir ilişki geliştirdik. Bu, kaydedilen akustik emisyonu karşılık gelen bir sıcaklığa dönüştürerek sıcaklığı etkileyen mevcut ömür modellerini kullanarak yaşam süresini değerlendirmemizi sağladı.

Anahtar Kelimeler: Elektortermal Model, IGBT, Akustik Model, Güvenil

To My Family

ACKNOWLEDGEMENT

I wish to start by thanking my thesis advisor Asst. Prof. Dr Canras Batunlu, department of Electrical & Electronics Engineering at the Northern Cyprus Campus of the Middle East Technical University. Asst. Prof. Dr Canras Batunlu was always available when I came across a trouble spot or was concerned on my thesis work. He permitted the research work to be my work consistently, but he always kept on the correct path whenever he thought there was a need. Finally, I should like to point out my most profound appreciation to my parents (John Ondieki and Daphine Nyaboke), my siblings (Amos Ratemo, Josphat Mugambi, Hesbon Ondieki), my friends and girlfriend (Molly Sharon, Joshua Mugisha, Bienevue Christian Bunani, Melvis Wanjiru, Anne Okello, Arthur Ngugi, Christabel Atieno) for giving me continued backing during my period of study and the research work and finally the write-up process of this thesis. Without them, the realization of this work would not have been possible.

TABLE OF CONTENTS

ABSTRACT v
ÖZ vi
ACKNOWLEDGEMENT viii
LIST OF FIGURES xi
LIST OF TABLES xiii
LIST OF ABBREVIATIONS xiv
CHAPTERS
1. INTRODUCTION 1
1.1 Research Scope 1
1.2 The Role of Power Electronics in Renewable 2
1.3 Research Motivation 3
1.4 Review of Related Literature 4
1.4.1 Failure in power electronic devices 4
1.4.2 IGBT Failure Classification 5
1.4.3 Reliability of power electronics 7
1.4.4 Monitoring 8
1.4.5 Ways of Determining the State Of Health of Power Modules 10
1.5 Research Objectives 10
1.6 Thesis Outline 11
2. HEAT MODELLING IN SEMICONDUCTORS 13
2.1 Thermal-Impedance Theory 15
2.1.2 Foster Model 16
2.1.3 FEM Method 16
2.2 Accelerated Cycling Tests 17
2.3 Accelerated aging experiment process 18
2.3.1 Initializing Stage 18
2.3.2 Heating Stage 18
2.3.4 Cooling Stage 19
2.4 Lifetime Analysis of Power Electronic Converters (PECs). 19
2.4.1. Empirical Lifetime Models 20
2.4.2 Physics-Based Lifetime Models 20

2.5 Thermal Response Analysis by FEM........ 21
2. 6 Temperature Distribution of Single Chip Model........ 23
2.7 Temperature Distribution of Single Chip Model in Surrounding Air........ 25
2.8 Thermal Modeling of PECs in Wind and Solar Energy Applications........ 26
2.9 Chapter Summary........ 27
3. ACOUSTICS MODELING........ 28
3.1 Acoustic Emission........ 28
3.1.1 Acoustic Emission Types........ 29
3.1.2 Sensors........ 32
3.1.2 Measurement Challenges and Sensor Performance........ 32
3.2 COMSOL Simulation........ 33
3.2.1. Sound Pressure Level........ 33
3.2.2 Acoustics of Single Chip Model........ 34
3.2.3 Acoustics of Single Chip Model in Surrounding Air........ 36
3.2 Chapter Summary........ 37
4. SIMULATION MODELLING RESULTS AND DISCUSSION........ 38
4.1 Reliability Modeling and Lifetime Analysis........ 49
4.2 Lifetime Analysis for Discrete IGBT Devices........ 51
4.3 Chapter Summary........ 55
5. CONCLUSIONS AND FUTURE WORK........ 56
5.1 Summary of Research Findings........ 56
5.2 Scope for Future Research Direction........ 57
REFERENCES........ 58
APPENDICES........ 63

LIST OF FIGURES

FIGURES

Figure 1.1 Wire bond Liftoff....6
Figure 1.2 Solder Fatigue....7
Figure 1.3 Deteriorated Power module....10
Figure 1.4 Thesis Methodology....12
Figure 2.1 IGBT Assembly and CTE of Each Layer with Different Materials....14
Figure 2.2 Simplified Representative View of the IGBT Module....15
Figure 2.3 IGBT Aging Test Flow Chart....19
Figure 2.4 Meshed Image of the Model IGBT....22
Figure 2.5 Heat Distribution at 0 Seconds....24
Figure 2.6 Heat Distribution at 400 Seconds....24
Figure 2.7 Heat Distribution at 800 Seconds....24
Figure 2.8 Heating Curve....25
Figure 2.9 Heat Distribution at 0 Seconds....25
Figure 2.10 Heat Distribution at 400 Seconds....26
Figure 2.11 Heat Distribution at 800 Seconds....26
Figure 2.12 Heating Curve in the Air....26
Figure 3.1 Acoustic Measurement Experimental Setup....28
Figure 3.2 Three Types of Recorded Acoustic Emissions....29
Figure 3.3 Acoustic Signals....31
Figure 3.4 Examples of Sensors for the Wide-Band Acoustic Emission. Two KRNBB-PC Sensors on the Left and One Kistler Piezotron Sensor on the Right....32
Figure 3.5 Sound Pressure Level Distribution at 30,000Hz....34
Figure 3.6 Sound Pressure Level Distribution at 45,000Hz....34
Figure 3.7 Sound Pressure Level Distribution at 60,000Hz....34
Figure 3.8 Graph of Sound Pressure Level against Frequency....35
Figure 3.9 Sound Pressure Level Distribution at 30,000Hz....36
Figure 3.10 Sound Pressure Level Distribution at 45,000Hz....36
Figure 4.1 Physical View of the Module....40
Figure 4.2 Acoustic Pressure Distribution at 10 kHz with A 75W Heat Source....41
Figure 4.3 Acoustic Pressure Distribution at 50 kHz with A 75W Heat Source....41

Figure 4.4 Acoustic Pressure Distribution at 100 kHz with A 75W Heat Source 41
Figure 4.5 Sound Pressure Level from 10000Hz to 90000Hz at 75W 42
Figure 4.6 Sound Pressure Level from 1000Hz to 10000Hz at 75W 43
Figure 4.7 Sound Pressure Level from 1000Hz to 9000Hz at 75W 43
Figure 4.8 Sound Pressure Level from 10Hz to 9010Hz at 75W 44
Figure 4.9 Sound Pressure Level from 10000Hz to 100000Hz at 75W 44
Figure 4.10 Sound Pressure Level from 10000Hz to 100000Hz at 75W 45
Figure 4.11 Sound Pressure Level from 10000Hz to 100000Hz at 75W 45
Figure 4.12 Sound pressure (dB) against Frequency 46
Figure 4.13 Relationship between Heat and Temperature 47
Figure 4.14 Relationship between the Sound Pressure Level and Heat 48
Figure 4.15 Relationship between Sound Pressure Level and Temperature 48
Figure 4.16 Relationship between Sound Pressure Level and Temperature 49
Figure 4.17 Graph of Temperature against Time 52
Figure 4.18 Number of Cycles against Mean Temperature and Temperature Deviation 53
Figure 4.19 N_f against Mean Temperature and Temperature Deviation 54
Figure A.1 IGBT Model in Air Showing the Different Probe Points 66
Figure A.2 30000Hz to 60000Hz (75W) 68
Figure A.3 3000Hz to 6000Hz (75W). 69
Figure A.4 300Hz to 600Hz (75W). 69
Figure A.5 30Hz to 60Hz (75W). 70

LIST OF TABLES

TABLES

Table 2.1 Material Properties..23
Table A.1 Sound pressure level from 10 kHz to 100 kHz at 75w 63
Table A.2 Sound pressure level from 10 kHz to 100 kHz at 75w 63
Table A.3 Sound pressure level from 10Hz to 9010HZ at 75w.................................64
Table A.4 Sound pressure level from 10kHz to 90kHZ at 75w.................................64
Table A.5 Sound pressure level from 1 kHz to 9 kHz at 75w 64
Table A.6 Sound pressure level from 1 kHz to 10 kHz at 75w 65
Table A.7 Sound Pressure Levels at Different Strategic Positions of the Chip.........67
Table A.8 Heat (W) against Temperature (degC)..70
Table A.9 Heat (W) against Sound Pressure Level (dB). 70
Table A.10 Temperature (degC) against Sound Pressure Level (dB)........................71
Table A.11 Sound Pressure Level against Temperature (deg C). 71
Table A.12 Temperature (degC) against Sound Pressure Level (dB)........................71
Table A.13 Relation between Number of Cycles Mean Temperature and Change in Temperature 71
Table A.14 Determining the value of Nf 71
Table A.15 Relationship between Nf Mean temperature and Change in temperature 73

LIST OF ABBREVIATIONS

ABBREVIATIONS

AC	Alternating current
DC	Direct Current
CM	Condition Monitoring
CSP	Concentrated solar power
DC	Direct current
Gtoe	Gigatonne of oil equivalent
HRES	Hybrid renewable energy sources
IGBT	Insulated gate bipolar transistor
MPPT	Maximum power point tracking
MW	Megawatt
PV	Photovoltaic
PWM	Pulse width modulation
RES	Renewable energy systems
CTE	Coefficient of thermal Expansion
PEC	Power electronic Converter
PC	Power Cycling
TC	Temperature Cycling
POF	Physics of Failure
FEM	Finite element Modelling
FEA	Finite element Modelling
V_{CE}	Collector Emitter Voltage
dB	Decibel
T	Temperature
t	Time
FIT	Failure in time

CHAPTER 1

INTRODUCTION

This chapter starts off the research work through the introduction of power electronics, particularly IGBTs, into the subject of study. Secondly, it explains the reasons behind this particular work, taking into account the benefits of the proposed approach. Then, the chapter outlines the study goals and the analysis procedure to be adopted in this dissertation. In the following sections, the information flow is represented as a review of the other studies.

1.1 Research Scope

The world energy consumption continues to increase at an average annual rate of 3.3%. The installed capacity will rise from 4400 (Gigawatts) GW (2007) to 6700 GW (2020) by more than 50 % by 2020. For 2030 the electricity generation capacity built will increase by 100% while worldwide demand for primary energy will rise respectively by just 55%. This implies a new annual of 150 to 200 GW installations[1]. Both fossil and nuclear sources currently supply the world's electricity. Such sources are still crucial for energy supply for the next few decades, given the rising issues of scarcity of available resources and environmental pollution. Such sources are, however, likely to be less accessible and of interest to the community. Alternative or sustainable sources of energy that are not dependent on carbon-based fuels and have a moderate impact on the environment, allowing meeting the increasing global demand for energy and reduction in emissions. Advanced sources of energy, such as micro-hydroelectric turbines, Wind turbines, PV, hydrogen fuel cells, wave and tidal energy technologies, aim to fulfil renewable energy needs. Such services are making a significant portion of the power grid recently. Incorporating these new advanced sources into the current electricity network will provide higher quality, reliable power to customers. Usually, the power produced by such sources of energy is not regulated or connected directly to the grids or properly in grid-based loads. Then it needs to be converted into a suitable kind, using electronic converters, irrespective of the power ratings of the substitute generating unit[2].

1.2 The Role of Power Electronics in Renewable

Sources of renewable energy in power systems have lately played a vital part in the production of electricity. Access to low-cost, environmentally sustainable energy is essential to the future economically of countries worldwide [3]. Therefore, reducing Carbon dioxide (CO_2) emissions requires the introduction of more renewables and less reliance on conventional fossil fuels [4]. The development of Power Electronics has matured substantially. After many years of the rapid growth of power semiconductor components in devices like inverters and converters. Power electronics components are mainly used for the transformation and regulation of electrical power using power semiconductor devices which operates in switching mode; making their efficiency to be as high as 98–99 per cent[4][5]. With the advancement of technology, reduced power electronics costs and their increased performance, power electronics are being utilized in various sectors including manufacturing, business, domestic housing, aerospace, military, utility and transport systems [6].

Furthermore, the use of power electronics on renewable energy systems (RES) are essential in the solving of our current energy shortages, as it enables efficient production, use and distribution of power by dramatically considering their high energy conversion efficiency [7]. Power electronics are required in most types of renewable energy systems. They are utilized for the monitoring of the source of renewable energy and the load interface, which can be connected to the grid or standalone. Power will, of course, flow bi-directionally, dependent on the topology and the application.

Electrical converters for RES are primarily used to control the inconsistent input power to optimize the energy produced by the systems. Inverters in the RES are used to transform DC voltage effectively to AC Voltage or to incorporate the power generated into the electrical grid [8]. Solar PV panels or wind turbines rely on the environments in which they work to generate electrical energy. Systems that incorporate solar and wind technologies produce power more effectively and are referred to as hybrid systems. These hybrid systems can be used either as standalone systems or be connected to the grid. When both sources are non-existent, no power will be produced. Energy storage is available in standalone systems to bypass this problem, thereby being able to provide energy during these periods of the non-existence of wind or sun[9]. Considering, power electronics converters are one of the critical

components of the network for the incorporation of renewable energy grids, investment in this direction would increase the uptake of renewable energy[10]

1.3 Research Motivation

The environmental impact of power electronics has traditionally been regarded as linked to acoustic and electromagnetic emissions, and it should be observed that in recent years the effect of electronics on the environment has been apparent. Owing in large extent to global regulations, standards and recommendations which were introduced, and also to the fact that these inverters and converters were processing much power, the electromagnetic emissions from power-electronics already became a significant issue during the last ten years of this century. It results in high pollution. The situation regarding materials and processes impact on the environment may evolve analogously, as the processes for regulating this for the electronics and electrical industry are already in place in several countries. Power electronics are vastly used across industries, and approaches would have a significant effect on technology growth and prices.

In terms of Reliability and environmental aspects of power electronics at the end of the design stage traditionally comprehensive testing, reviews and corrective steps were taken immediately required should particular problems occur [11]. This has now changed dramatically both because these aspects were taken into account in earlier design stages and because green technologies in the industry have become trendier. In designing durable and reliable power electronics devices, the efficiency of all energy systems in production environments has tremendously improved. The technology does, however, at the same time include a significant environmental impact. In addition to active (silicon, SiC and GaN components), aluminium, copper and its alloys contain bulk metals which provide significant mechanical, thermo-electrical and the packing of electronics[12].

1.4 Review of Related Literature

1.4.1 Failure in power electronic devices

Power electronic converters being widely used society; low power converters are found in power supplies of computers, mobile devices, and lighting applications[13]. But an average user is possibly using hundreds of power converters every day without understanding what they are. For many industrial applications, higher-power converters can be used, including electrical drives, renewable electricity generation, and even the energy grid for the future [14]. In the case of an unanticipated fault, the plant operation is interrupted and, in frequent cases, a risk of harm or injury is present. There can be high financial costs as well: beyond the immediate maintenance expense, an interruption in output leads to a loss in revenue. The expense of lengthy unplanned disruption, for example, for offshore wind turbines, can be incredibly costly because of the difficulties of reach to site area[15].

Several electronic components, including the Insulated Bipolar Gate (IGBT), are utilized in DC-DC converters and DC-AC inverters. An IGBT has a comparatively shorter service life than other electronic converter parts. IGBTs are hybrid semiconductors for bipolar-metal-oxide with the benefits of low resistance, gate voltage control and large secure operating area[5]. The commonly used power electronic components for manufacturing applications are IGBTs. IGBTs are vital components and are widely used power devices[16]. The failure of IGBT and the approaches to boost the efficiency of IGBT electronic power converters are also worth investigating. It is due to thermal, mechanical impacts, long-term exposure and a complex mission profile to high temperatures. IGBTs are made up of various layers with different Properties. Heat is transmitted from the chip to the cooling system using different heat paths, with temperature variations within the layers, caused through a thermal cycle. Therefore, stress occurs in connected materials with various thermal expansion coefficients. It causes fatigue in different power module locations such as bonding wires, solders and failures. IGBT failure can generally be grouped as a catastrophic failure or wear-out failure. The failure to wear the IGBT is mainly caused by the accumulation of degradation over time, while a single event causes disastrous failure due to stress, such as over tension, current and overheating [17]. The Prognostics and Health Management (PHM) system will track the deterioration of IGBTs and predict wear-out failure. Though, for catastrophic failure, PHM is not appropriate, which is harder to predict[18][19].

1.4.2 IGBT Failure Classification

IGBT failures are grouped as open circuit (OC) and short circuit (SC) failure. OC failure for converters is not generally seen fatal as the Converter will be able to function though with lower output quality. In comparison, short-circuit failures on converters are almost disastrous, as the uncontrolled short-circuit current ruins the failed IGBT and other circuit elements. [18][20].

1.4.2.1 Open-circuit Failure

IGBT open-circuit failures can occur due to vibration after external disconnection, as well as the lifting and breaking of the bonded wire due to high, short-circuit current, as shown in figure 1. This may lead to the pulsating current, distortion of output current/voltage, and secondary failure after a given period of different components. Even the lack of a gate drive signal can cause an open-circuit. Driver part damage and disconnection between the driver board and the IGBTs may be common causes. The IGBT open-circuit failure is not necessarily catastrophic but can cause other devices and the Converter to fail secondary. Below are the reasons for failure [18].

1.4.2.2 Bond wire liftoff

After short-circuit failure, bond wire liftoff failure may occur. It is generally due to technical factors. It is mainly caused by the different coefficient of thermal expansion (CTEs) between silicon and aluminium, along with high-temperature gradients [21]. The crack starts at the edge of the bond interface, and the crack slowly rises as it reaches the weakest central bond region. The main emitter binding wires usually fail first, and the survivor binding wires fail. A bonding wire crack that is slower than the lift is also causing failure and is typically observed after long cycle power tests [22].

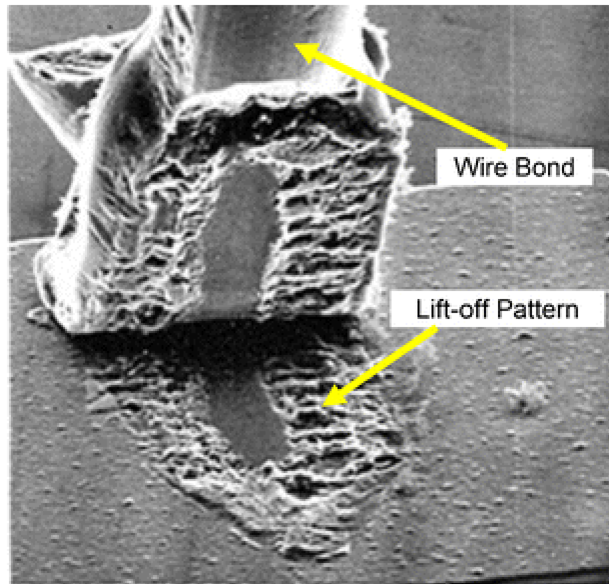

Figure 1.1 Wire bond Liftoff

1.4.2.3 Solder Fatigue

High-temperature variations affect soldered joints strength due to the creation of cracks and fatigue processes, which ultimately lead to failure. Due to the changes in the thermal expansion of the solder joints such as silicone and cotton, this failure occurs [23]. This layer has high shearing stress which fails due to inconsistent thermal expansion coefficients (CTE) layers and temperature gradients. This would ultimately result in cracks leading to a significant reduction in heat transfer and a substantial rise in dietary heat. This is due to fatigue[22].

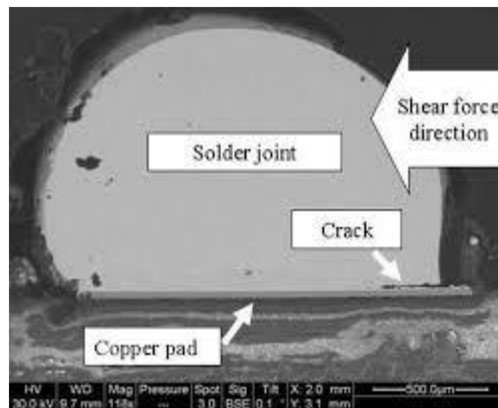

Figure 1.2 Solder Fatigue

1.4.2.4 Short-circuit Failure

The high gate voltage and external failure of IGBT short circuit will trigger during turn-on. Due to static latch-ups, or exponentially increasing intrinsic Temperature caused by a second collapse, or by power shocks, failure while in the state[24]. Dynamic latch-up and high voltage failure can be triggered during switch-off. A thermal runaway phenomenon can trigger Off-state failure[18][20].

1.4.3 Reliability of power electronics

As described above, power electronics has many applications, including consumer electronics, industrial plants, traffic, and electric power generation and transmission. In several of these situations, condition monitoring will help the plant operator to handle problems of Reliability and improve the efficiency of the plants[25] [26]. Wind energy, as an example in a Finnish wind power plant in 2010 A cumulative shutdown of 6219 hours, accounted for 13.1 per cent of the overall shutdown time, triggered the power electronics fault. In the Swedish survey, in 14.3 per cent of cases, the electrical device, except the generator, was the cause of failure. A significant proportion of faults are caused by power semiconductor devices, particularly power transistor modules. Statistically, in 19 percent of

the power converter faults, a power semiconductor failure was reported as the cause of converter failure[27].

In the early stages of product development, the reliability of IGBTs is typically tested by physical tests such as power Cycling (PC), Temperature cycling (TC) and vibration tests. The test-analysis-fix cycles are, therefore, costly and time-consuming. During the design process, POF-based evaluation was generally accepted as an effective and economical way of ensuring reliability. Because of the continuous development of the IGBT modules, the failure rate fell from 1000 FIT (failure-in-time:failures in a billion hours) in 1995 to 20 FIT in 2000 and a few FITs in recent years[28]. The failure rate is dependent on temperature stresses such as the mean temperature, and temperature deviation thereby varies from case to case and mostly tested using the PC and TC tests[29].

The method of condition monitoring assists the machine user by cutting down on downtime due to failure. Power electronics is the right candidate in wind power systems for condition monitoring, as failures associated with it appear to cause relatively extended downtime in wind power systems, and failures in power electronics are the most common form of failure[30].

For solar power systems, plant owners allow the electronic power converters to have 20 years of working life. Current power converters can maintain this life span, and future advances in power semiconductors and packaging are expected to prolong the converters' life even further. Even in that situation, a condition monitoring program will boost the Converter's user experience near the end of life[31].

1.4.4 Monitoring

Condition Monitoring (CM) is a method or mechanism for tracking a physical system's operating characteristics such that a change in the monitored characteristics can be used to plan maintenance before a significant deterioration or breakdown [32]. CM requires knowledge of individual part or integrated device failure mechanisms, sensor technology, data collection and analysis, and the capacity to estimate the system's health status [33].

There is currently no commonly accepted procedure for tracking power electronics conditions. Most of the proposed methods are based on the Power Transistor collector-emitter voltage calculation. This system is capable of detecting impending bond-wire lift

faults but is unable to identify failures triggered by other mechanisms. Additionally, the voltage-based state estimator requires a voltage calculation on each transistor to be performed separately[34].

As well as calculating the voltage from the collector-emitter, turn-off time was suggested as an indication of failure. It was also indicated that the Gate Circuit be a source of knowledge on condition control. Nonetheless, both approaches require very rapid measurements of the voltage on each transistor.

Due to a still inadequate association between documented deterioration or incipient failure and measured physical states, the application of the CM principle to power electronics is difficult.

The former needs more understanding of mechanisms for device or system failure, and the latter includes realistic strategies for tracking performance degradation. Condition tracking will reduce the situation considerably by allowing operators to schedule preventive services to converters. There is currently no commonly accepted early warning system available for errors, however [33].

Acoustic emissions have been used in several applications as a condition monitoring device; the best known of which is possibly bearing failure detection and rotational machine monitoring. Specific examples include tracking of pipeline conditions, concrete structures, steel pipes and equipment, and monitoring for corrosion [35].

For electronics, some research has been done on capacitors where acoustic emission in semiconductor components was correlated with partial discharge, and acoustic emission in light-emitting diodes has been studied. Structural variations in the semiconductor material responsible for changes in the spectrum of emitted light have also been shown to cause acoustic emissions [36]. The acoustic signals in the control module are minimal in the power semiconductor modules, and the plastic parts in power modules cause substantial damping.

1.4.5 Ways of Determining the State Of Health of Power Modules

1.4.5.1 Scanning Acoustic Microscope (offline)

Acoustic microscopy scanning is an image-based approach which could be used to identify faults in the layers of chip weld. Figure 3 shows a deteriorated Power module which scans multiple module layers without damaging the architectural design of the chip. That type's downside is the need to detach the module from the circuit[37].

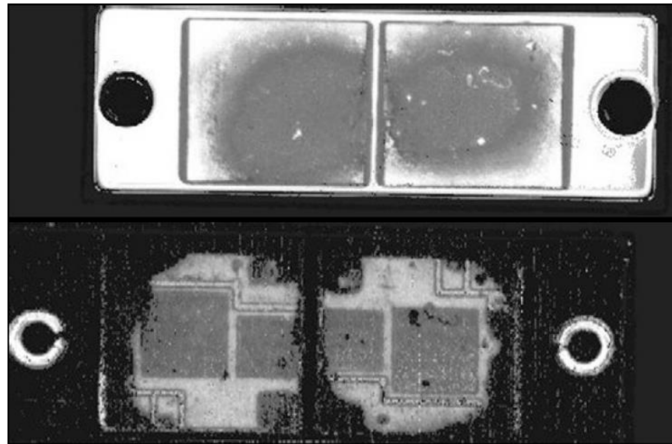

Figure 1.3 Deteriorated Power module

1.4.5.1 Measurement of V_{CE} (T) (offline)

The Temperature of the chip is measured using method V_{CE} (T). The V_{CE} (T) method can be used as a Semiconductor degradation predictor. The lifespan of the power module can also be calculated based on those measurements. The V_{CE} (T) approach is ideal for detecting lift offs and deterioration of chips from the bond wire. This method is primarily used in power-cycling research[37].

1.5 Research Objectives

In recent decades, there has been an increased use of power electronic devices, especially renewables due to the uptake and push for clean energy technologies to reduce the effects of

climate change. The main focus of the thesis is to increase the reliability of power electronic devices by looking into the acoustics generated by the IGBT chips in the power electronic components (PECs) of the renewable energy systems. Therefore, the objectives of the study are outlined as follows,

- What's the relationship between acoustics and Temperature generated in semiconductor devices?
- Proving the acoustic emission phenomenon in IGBTs by use of simulations. Then look into its effects on the long-term Reliability of the IGBTs and diodes (Semiconductors) in the Solar/Wind inverter system.
- Can we use acoustics as a way of monitoring the health of semiconductor devices?

1.6 Thesis Outline

The literature reviews on heat Finite Element Analysis (FEA) simulations and IGBT experiments on regards to heat will be discussed in Chapter 2. Chapter 3 will address literature reviews on acoustic FEA simulations and IGBT experiments on regards to acoustics. Chapter 4 describes the methods used by the simulation program COMSOL Multiphysics and the results of the model, and Chapter 6 provided the conclusions of the study and suggestion that future research is needed to enhance this study. Figure 1.4 below represents the outline flow.

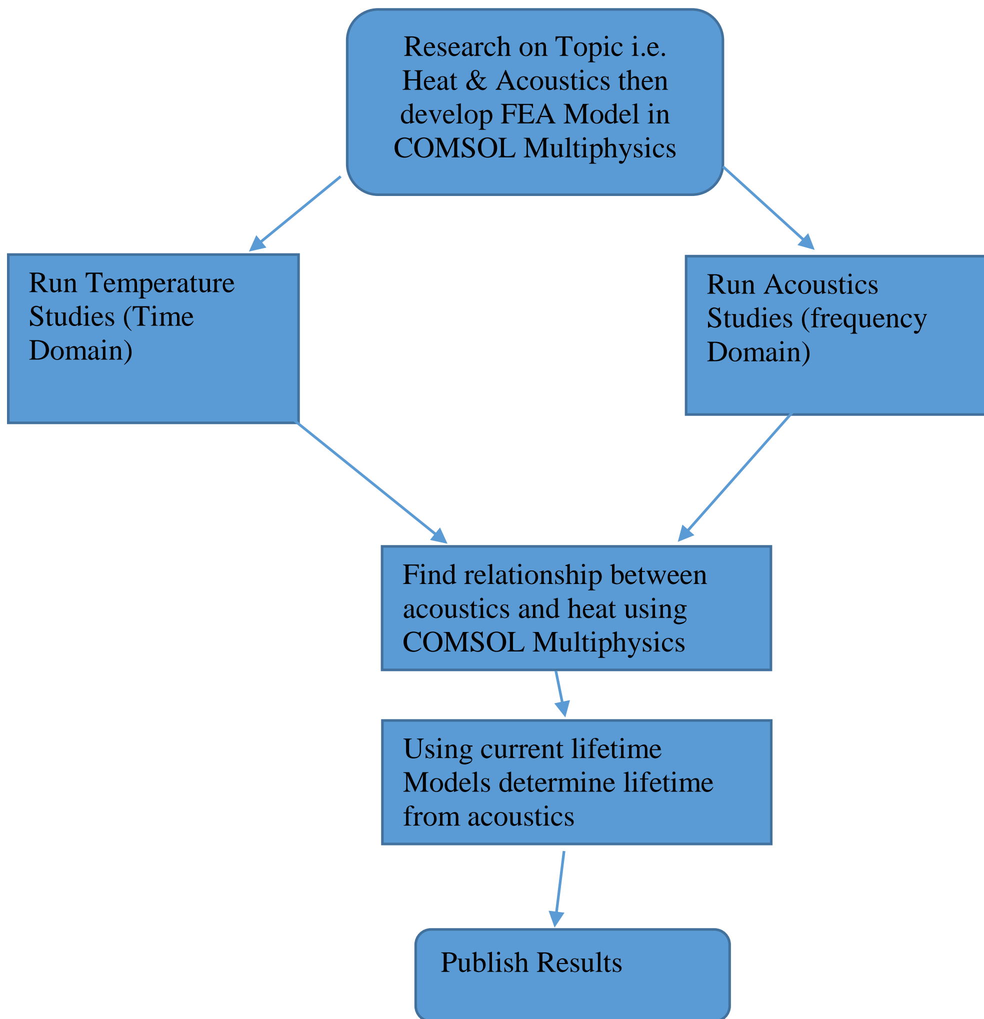

Figure 1.4 Thesis Methodology

CHAPTER 2

HEAT MODELLING IN SEMICONDUCTORS

By one of three processes, conduction, convection or radiation, heat may be transferred from one material to another. Conduction takes place when two components have direct contact between them, and convection happens when the content is surrounded by gas or fluid. Radiation is heat loss from the atmosphere by infrared light radiation [38]. In practical use, IGBT modules are cooled by placement on a heat sink, natural air cooling or forced air cooling. The heat generated within the IGBT module can also be transmitted into the air or radiated directly into the air by means of convection (air cooling) — both operating output and service life are affected by the IGBT module operating Temperature. A standard error is an assumption that the continuous thermal resistance of the junction is constant. The thermal strength of the interconnecting case depends on the heat present, the state of the heat sink and the temperature of the environment [39].

Owing to the dissimilar coefficient of thermal expansion (CTEs) of layers for IGBT modules, repeated thermal-mechanical stress causes solder fatigue often occurring in the form of voids, cracks and even layer delamination [40][41]. The defects can be observed in soldering from the base plate to the ceramic substratum and in welding from the silicone chip to the ceramic substratum. Usually, soldering fatigue increases heat flow density and reduces heat dissipation. This results in their temperature junction and thermal resistance. Statistics show that > 55% of failures in IGBTs comes as a result of temperature conditions. The failure rate almost doubles with every 10 ° C in the operating environment. In practice, to prevent possible defects, the mean temperature of the junction must be between the maximum permissible and the minimum temperatures usually below 125 ° C [42]. Several studies have been conducted from thermal stress to explore the thermal stress criteria in the assessment of health conditions [43]. IGBT structure and CTE of each layer with different materials are shown in Figure 2.1

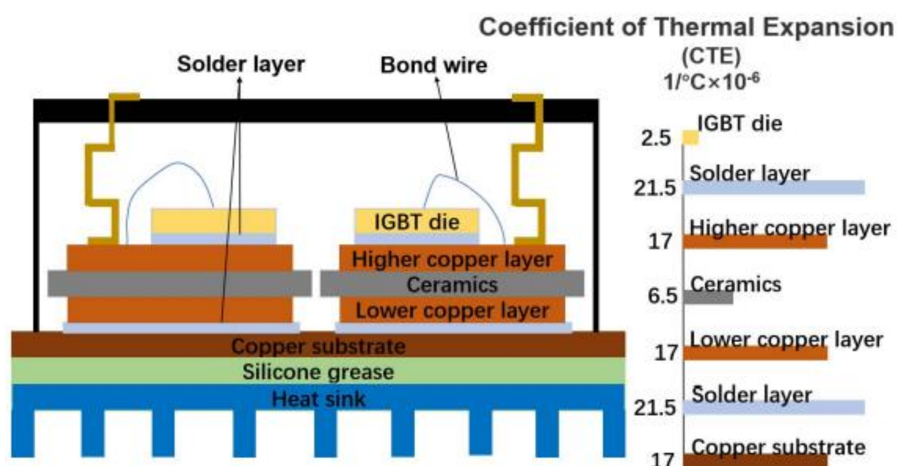

Figure 2.1 IGBT Assembly and CTE of Each Layer with Different Materials

Most thermal analysis is carried out with continued thermal resistance over the entire life period of the system, making the solder layer degradation process for lifelong evaluation to be overlooked. The resistive model is based on specified thermal parameters derived from the datasheet or initial testing performance of the manufacturer's power module [44]. For thermal modelling, the actual thermal load of the IGBT module shall be understated until it is aged if thermal resistance does not increase with the degradation level. Thermal stress degradation of the solder material would increase thermal resistance, thus increasing the thermal fluctuation of IGBT assembly. The fatigue feedback effect, particularly in the later period of its operating life, must be considered for the assessment of the Reliability of the device [45]. The simplified representative view of the IGBT module studied is shown in Figure 2.2.

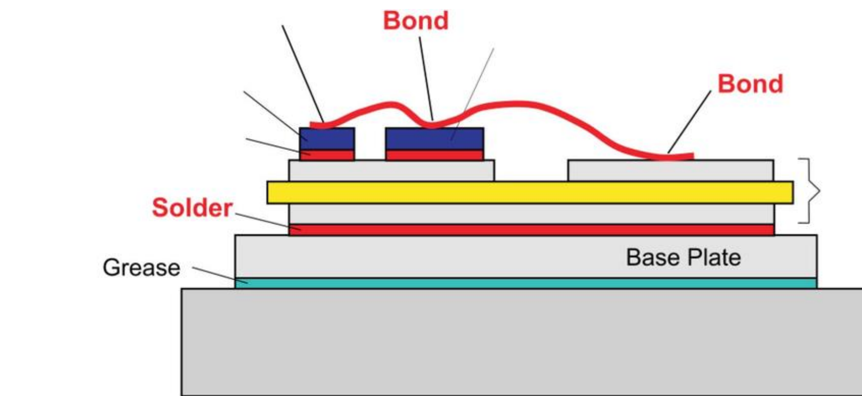

Figure 2.2 Simplified Representative View of the IGBT Module

2.1 Thermal-Impedance Theory

Usually, thermal impedance is given by a network of thermal resistance and RC thermal capacitance. The RC network can then be implemented in various simulators with specific thermal aspects. As mentioned below, there are two styles of widely used versions, i.e. Cauer and foster models [39].

2.1.1 Cauer Model

Cauer thermal impedance model is related to the geometry and physical characteristics of the different IGBT modules[46]. It is possible to measure the thermal resistance R_{th} and thermal capacitance C_{th} of different physical layers, e.g. chip solder as;

$$Rth = \frac{1}{k} \cdot \frac{d}{A} \tag{2.1}$$

$$C_{th} = C_p \cdot \rho \cdot d \cdot A \tag{2.2}$$

d = Thickness of the material.

A = Cross-sectional area.

k = Thermal conductivity.

ρ = Density.

c_p = Specific heat capacity.

2.1.2 Foster Model

The Foster model defines an IGBT module's thermal behaviour as a "black box." "The model is typically implemented using the following exponential equation, based on the installation of a thermal reactions curve according to IEC Standard 60747-96.3.13:

$$Z_{th}=\sum_{m=1}^{n} R_{th_m}(1-e^{-\frac{t}{R_{th_m} \cdot C_{th_m}})}) \quad (2.3)$$

Z_{th} = Thermal impedance,

n = Total number of RC branches in the RC network,

R_{th_m} = Thermal resistance,

C_{th_m} = Thermal power [47]

2.1.3 FEM Method

The FEM approach is another conventional thermal analysis technique. Based on the materials and geometries of the IGBT module, the FEM approach can perform thermal appearance simulations without expensive hardware modifications and achieve efficient resource temperature and thermal impedance values. The basic concept is to solve the FEM diffusion-convection-reaction problem. In Fourier law, the heat transfer process can be defined when the heat flow is extracted from the conductivity and temperature gradient in a given direction,

$$q'' = k_i \nabla_i T(\underset{r}{\rightarrow}, t) \quad (2.4)$$

q'' = Heat flux.

k_i = Thermal conductivity.

T = Temperature.

$\underset{r}{\rightarrow}$ = Location information.

t = time.

The diffusion-convection-reaction equation can be derived by considering the situation as a flow problem and using energy conservation as,

$$\rho C_p \frac{\partial \mathrm{T}(\underset{r}{\rightarrow}, t)}{\partial \mathrm{t}} = \nabla . \left[k \, \nabla \mathrm{T}(\underset{r}{\rightarrow}, t)\right] + H \tag{2.5}$$

ρ = Density.

C_p = Heat capacity at constant pressure.

H = Heat.

k = Thermal conductivity which is assumed to be isotropic [48].

ANSYS / Icepak or COMSOL Multiphysics can be employed to solve diffusion convection-response equations, resulting in temperature knowledge of various IGBT modular layers. Therefore, a simplified Cauer or Foster model can be obtained based on temperature information [46].

2.2 Accelerated Cycling Tests

PECS requires long-term guarantees of up to five to 30 years, as in cars, locomotives and aircraft. Collecting system data for reliable assessment under real application conditions is not feasible as technology advances very quickly, and power module manufacturers need specific guarantees for new products. As a result, rapid Power and Temperature Cycling (PC &TC) tests are performed. Power module manufacturers are well known as a way to predict products for a lifetime[49]. PC and TC experiments are designed to accelerate failure modes which occur due to thermo-mechanical wear out in actual applications. Technical procedures for PCs and TC tests, such as set up current loads and cooling times, are mainly product-based and mostly defined separately from the manufacture. IEC International Semiconductor Standards, such as IEC 60747-34 and IEC 60747-9, require the implementation of performance and reliability measures. The effect of ambient temperature fluctuations upon power modules is calculated using temperature-controlled chambers. The main goal of these

steps is to determine possible weak points, such as the welding joints between the base plate and the power module substratum. During PC testing, the power module is continually heated by turning the current on and off, which results in different heat and cooling phases. This makes the device a source of heat dissipation and the device closures, i.e. the bonds and chip solder, are more strained and vulnerable to failure. Manufacturers' PC research is also used for power loss modules and for collecting useful life modelling data in the short term [50].

2.3 Accelerated aging experiment process

2.3.1 Initializing Stage

The IGBT case temperature TC is continuously collected by a control workstation with a data acquisition card. It determines whether the module is to be heated or cooled to the upper heating limit and the lower cooling limit, giving the control switch the correct control signal.

2.3.2 Heating Stage

A constant power supply with a current monitor helps to change the IGBT's current and peak current wavelength according to IGBT modules' working conditions. This modifies the shell temperature to the upper limit. The control switch activates the IGBT in the pulse current, and the intersection temperature rises. The control switch will be closed when the module shell temperature reaches the ceiling. For the determination of the degree of bonding wires fault, the VCE shall be collected during the heating process.

2.3.3 Ending Moment of the Heating

In the current 100 mA source, the VCE value of IGBT modules is reported and measured. As power consumption in IGBT is negligible at 100 mA, the combined temperature of T_c and T_j is assumed to be approximately equal at 100 mA. The temperature for the connecting shall be determined using the linear correlation between the junction temperature and the

VCE of 100 mA. Equation (6) extracts the Rth thermal resistance value to assess the degree of solder ageing [51].

$$R_{th} = \frac{T_j - T_c}{V_{CE}.I_c} \tag{2.6}$$

2.3.4 Cooling Stage

The temperature setting for the temperature box should be at least the same as that of the shell temperature of the measured module, which reaches the lower limit value if the IGBT signal switch is turned off. The box is closed, and the heating stage is reached. Reciprocation of heating and cooling leads to the accelerated ageing of the Power Panel. The failure criteria are a 5 per cent rise in the VCE decrease in saturation pressure and a 20 percent increase in R_{th} thermal strength as a module failure criterion [52]. IGBT aging test flow chart is shown in Figure 2.3

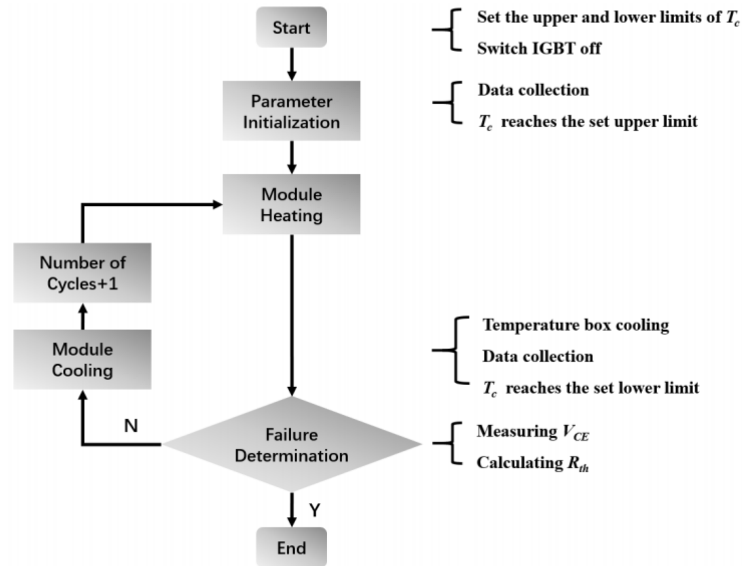

Figure 2.3 IGBT Aging Test Flow Chart

2.4 Lifetime Analysis of Power Electronic Converters (PECs).

The PECS is designed for high voltage alternating and blocking speeds. Subject to operational test conditions, power losses result in higher temperature fluctuations which, in turn, generate thermo-mechanical stresses within power modules that slowly degrade

functionality and cause usury. The power losses of PECS are determined in the first phase of life modelling using electrical circuit simulations for the characteristic load profile and transformed into acceptable temperature profiles which are subject to the modelling of the power module layers. In particular, thermal modelling and simulation are carried out in order to obtain knowledge and information on the tempering process in the power module system as direct temperature measurements of the power module layers are practically impossible. Because the electrical properties of the temperature-dependent switching equipment, e.g. power modules, will allow thermal-electrical simulations to determine the actual temperature behaviour accurately. The core concept of life modelling is the relationship between the number and temperature profiles of the failure cycles given directly in the PC and TC studies, namely N_f. This also tests the reaction of the power module to quantitative changes in operating temperature. Lifetime modelling of power modules is therefore very reliant on the results of cycle study. Life simulation methods widely used are statistical models and one of physical life.

2.4.1. Empirical Lifetime Models

Empirical models arise from shared data sets of PC test results collected over several years for various module technologies; they mark life-based on the number of fault cycles, N_f. The N_f depends on test parameters, such as maximum, average and minimum temperature, cycle length, heating and cooking time, loading current and the power module, such as the voltage and the wire link geometry. The impact of PC test parameters on the results of N_f is tested using a PC test. The predominant PC experimental failure mechanisms are attached wires and interconnected soldering layers, i.e. End of life (EOL) power modules, which are usually constrained by their lifetimes.

2.4.2 Physics-Based Lifetime Models

Physical modelling means that failure and deformation mechanisms are understood to model the strain and vibration output within the power module and to correspond precisely with the number of fault cycles. Physics of Failure (POF) work is focused on physical models. POF offers a clearer physical understanding of the process of failure observed and is thus a promising alternative to empirical life models. Precise stress and stress tests include the use

of high-resolution instruments, including infrared and electron microscopy scanning for electronic equipment. Within the Power Module, the other way of measuring stress deformations is by computer mechanics, such as a Finite-Element-Analysis (FEA) stress simulation. However, FEA modelling offers a thorough understanding of the material and nature of the power module mounting that is often not included in the power module datasheets. The FEA alternative for stress-strain modelling is a computational method for measuring stress-strain response using a parameterization technique based on the PC test results under the defined temperature profile [50].

2.5 Thermal Response Analysis by FEM

Usually, FEM simulations are used to determine the location of potential power module failures. [53]. Thanks to the Multiphysics Approach, a more realistic analysis of the characteristics of the modules can be done. Electro-thermo-mechanical domains are highly requested to simulate the performance of the system under real-time conditions for power module packaging. Specific Multiphysics models for the study of the deterioration and life of the wire and welding layer have been published. However, one of the difficulties is to take into account the developments in geometry, typically related to crack propagation anomalies in electronic power modules [54].

Thermal models are designed to explain the transient thermal behaviour of power electronics or converters during operation into estimated mean and varying temperature profiles. Two fundamental theorems described by Foster and Cauer are based on thermal modelling techniques. Foster models based on previously mentioned models with additionally improved RC thermal elements. The study of 3-D finite element modelling continued to develop until the late 1990s. The accuracy of such a model is high as the finite boundary condition for small sections of the material in the scaled components is overcome by the equation applied. These simulations do, however, require long-term, temporary thermal simulations for electronic power applications. Another solution may be the use of the Fourier Analytical Series to avoid the removal of the RC thermal equivalent circuit. The Finite Element Analysis (FEA) is a necessary means of tracking thermo-mechanical behaviour. Due to the heat source, IGBT is mainly caused by current losses, and the temperature change can lead to IGBT thermal stress and deformation of the module. For this function,

Multiphysics applications such as COMSOL, ABAQUS, ANSYS and SOLIDWORKS can be used to create a 3D hybrid, electrical-thermal-mechanical model.

The FE model of the IGBT single-chip module has been analyzed in-depth using COMSOL. The dimensions and material properties of each sheet as well as the geometric shapes of the wire bonds were explicitly designed to improve accuracy. The meshed image of the model inverter with the heat sink connected to it is shown in Figure 2.4

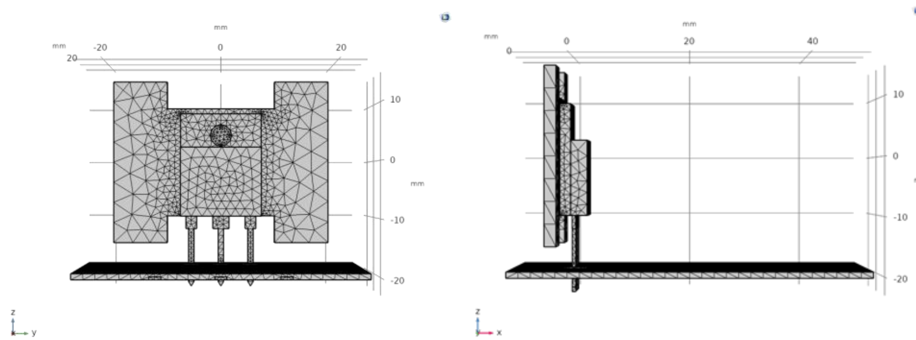

Figure 2.4 Meshed Image of the Model IGBT

Geometry was modelled with tetrahedral elements. The mesh size for the heat sink and the module's layers vary for computational efficiency. The mesh refining was completed by a two-scale factor, particularly for narrow binding edges and only thin welding layers. The thermal conductivity properties in the model are defined as a temperature function and considered a dynamic function. In order to solve the distribution of temperature variations, the heat diffusion equation was determined for the entire model [55]. It is defined as:

$$\frac{\delta^2 T}{\delta x^2} + \frac{\delta^2 T}{\delta y^2} + \frac{\delta^2 T}{\delta z^2} + \frac{q}{k} = \frac{\rho c}{k} . \frac{\delta T}{\delta t} \tag{2.7}$$

T = Temperature.

k = thermal conductivity.

C = specific heat.

ρ = Density.

q = Rate of energy production in covering the volume being studied.

The heat sink was not mounted on the board, and the silicone gel encapsulation was removed. Therefore, thermal insulation for the inverter board is no longer provided. The coefficient of thermal transmission h is specified as 5 W / m2 K over the model of the natural convection to ensure these conditions. Table 2.1 displays the thermal and mechanical properties used for FEM simulation.

Table 2.1 Material Properties

		Copper	FR4 (Circuit Board)	Solder, 60Sn-40Pb	Silicon	Material 10	AluminiumG	Gold
Electrical conductivity	S/m	5.998e7[S/m]	0.004[S/m]	6.67e6[S/m]	1e-12[S/m]	0.004[S/m]	3.774e7[S/m]	
Heat capacity at constant pressure	J/(kg·K)	385[J/(kg*K)]	1369[J/(kg*K)]	150[J/(kg*K)]	700[J/(kg*K)]	1700	900[J/(kg*K)]	
Relative permittivity	1	1	4.5	1	11.7	1	1	
Density	kg/m^3	8700[kg/m^3]	1900[kg/m^3]	9000[kg/m^3]	2329[kg/m^3]	900	2700[kg/m^3]	
Thermal conductivity	W/(m·K)	400[W/(m*K)]	0.3[W/(m*K)]	50[W/(m*K)]	130[W/(m*K)]	0.2	160[W/(m*K)]	
Relative permeability	1	1	1		1		1	1
Coefficient of thermal expansion	1/K	17e-6[1/K]	18e-6[1/K]	21e-6[1/K]	2.6e-6[1/K]		23e-6[1/K]	
Speed of sound	m/s	343	343	343	343	343	343	
Young's modulus	Pa	110e9[Pa]	22e9[Pa]	10e9[Pa]	170e9[Pa]	172*10^9	70e9[Pa]	
Poisson's ratio	1	0.35	0.28	0.4	0.28	0.25	0.33	
Reference resistivity	Ω·m	1.72e-8[ohm*m]		4.99e-7[ohm*m]]	3.48			
Resistivity temperature coefficient	1/K	0.0039[1/K]			0			
Reference temperature	K	298[K]						
Refractive index, real part	1				3.48			
Refractive index, imaginary part	1				0			
Murnaghan third-order elastic modu	N/m^2						-2.5e11[Pa]	
Murnaghan third-order elastic modu	N/m^2						-3.3e11[Pa]	
Murnaghan third-order elastic modu	N/m^2						-3.5e11[Pa]	
Lamé parameter λ	N/m^2						5.1e10[Pa]	
Lamé parameter μ	N/m^2						2.6e10[Pa]	

Temperatures for the ambient and heat sinks were set at 25 ° C. The chip was heated with 0.6W of the boundary heat source[56]. The Foster model represented transient thermal resistance r_{th} and thermal capacitance c_{th} for each layer.

2. 6 Temperature Distribution of Single Chip Model

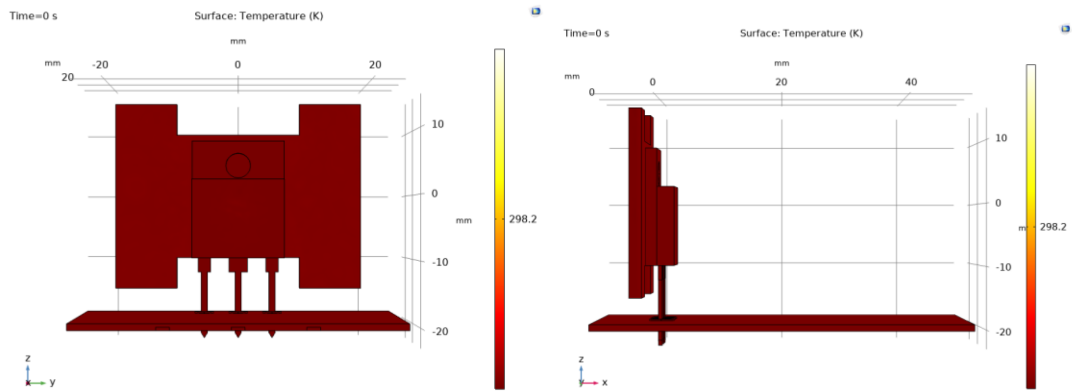

Figure 2.5 Heat Distribution at 0 Seconds

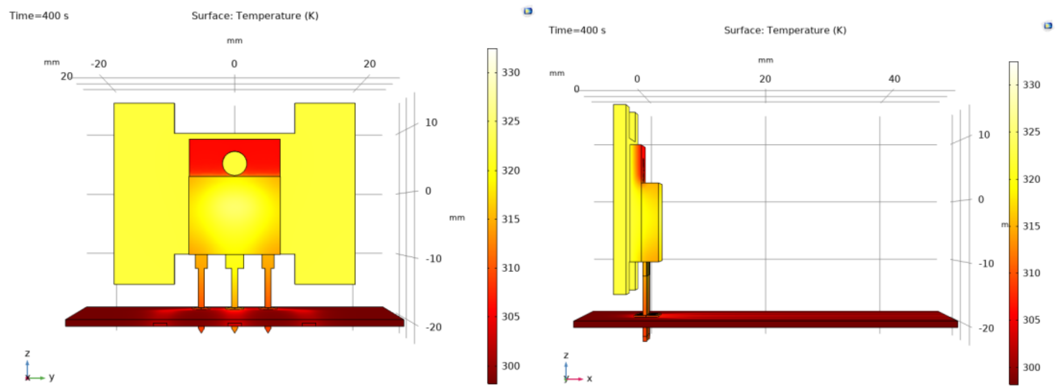

Figure 2.6 Heat Distribution at 400 Seconds

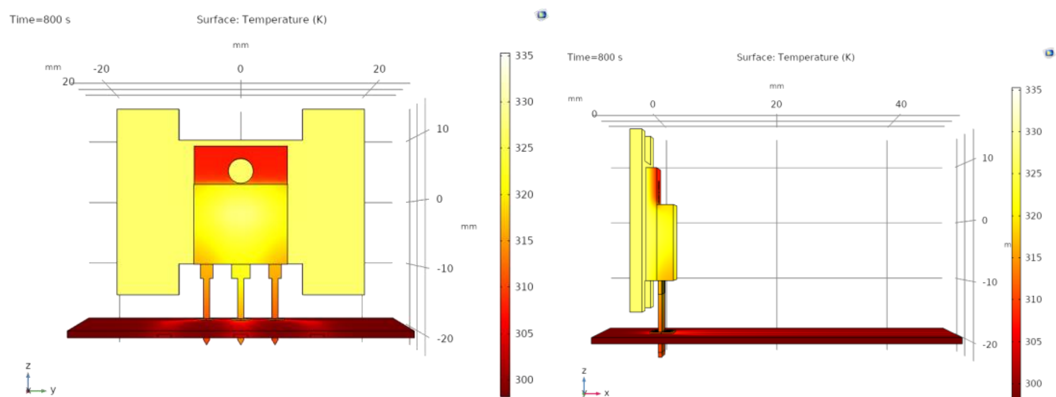

Figure 2.7 Heat Distribution at 800 Seconds

The simulation was used to create a thermal network computed until the heating curve's phase reaction enters a stable state [57], as shown in Figure 11.

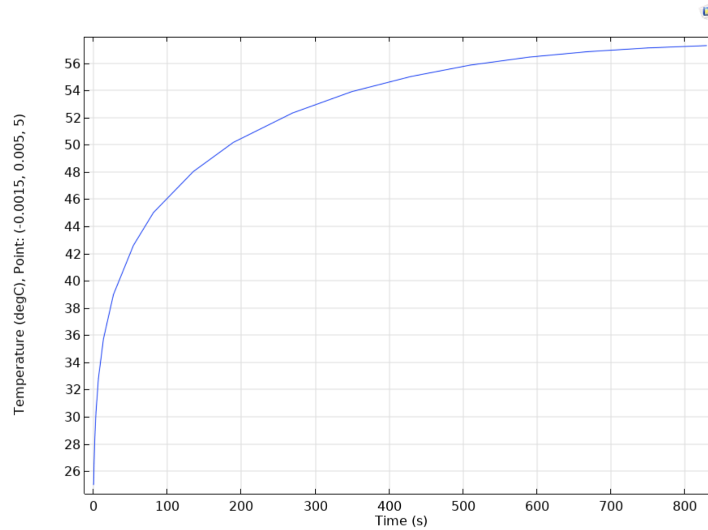

Figure 2.8 Heating Curve

2.7 Temperature Distribution of Single Chip Model in Surrounding Air

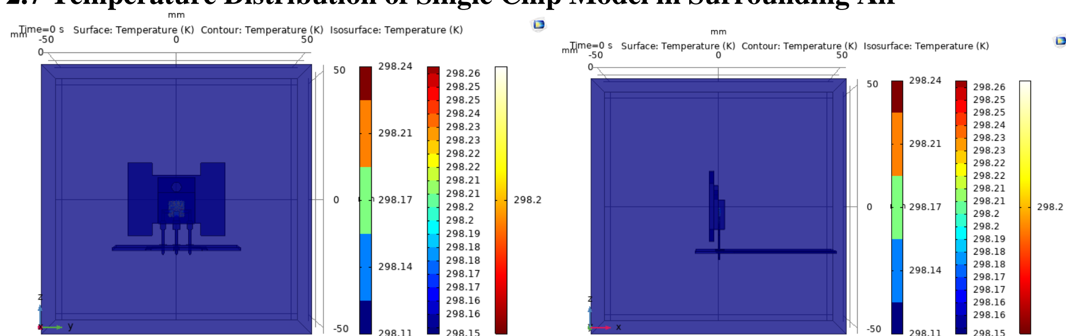

Figure 2.9 Heat Distribution at 0 Seconds

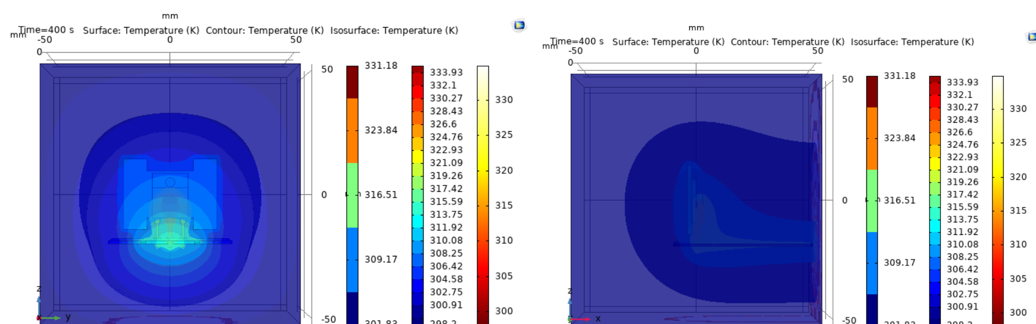

Figure 2.10 Heat Distribution at 400 Seconds

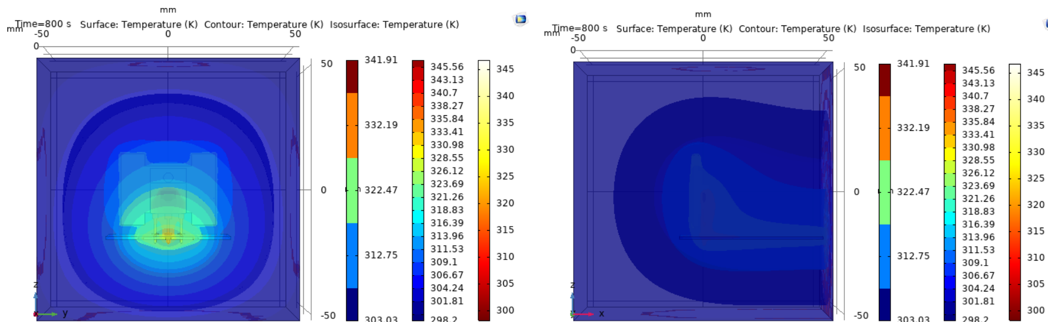

Figure 2.11 Heat Distribution at 800 Seconds

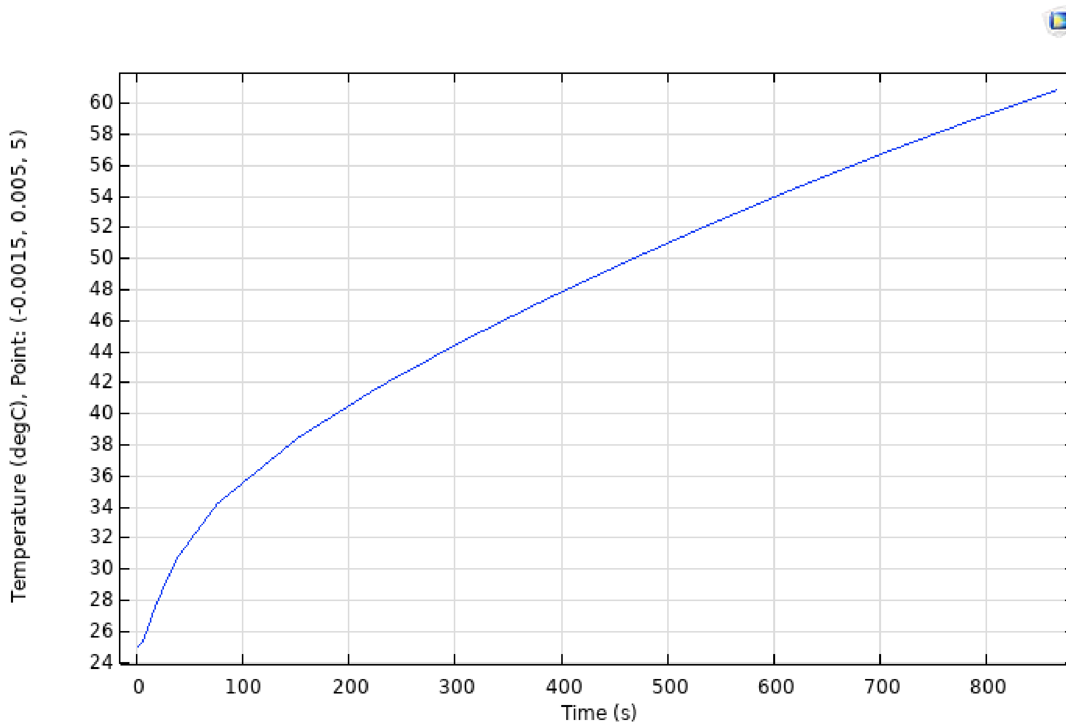

Figure 2.12 Heating Curve in the Air

2.8 Thermal Modeling of PECs in Wind and Solar Energy Applications

Wind and solar energy technologies have been two major clean energy advances that are rising the most. The reliability and life of these systems depend heavily on the PECs. They suffer from problems of reliability caused by erratic and robust wind, radiance rates and

variations in load [58]. Due to their ease of movement and higher frequency switching capacities compared with other semiconductor devices, extensive applications of bipolar insulated transistors (IGBTs) have been found in PECs. PEC malfunctions in renewable energy systems causing electrical/control system failure and leading primarily to failure. The DC bus voltage control is already sufficient for the maximum power point tracking (MPPT) in either solar or wind systems for renewable energy, thus avoiding distorted power generation and grid interfaces [34]. A DC voltage control system was developed previously for a back-to-back converter which is connected to a variable speed wind turbine [59]. The basic purpose of these control systems is to maintain a constant DC voltage. However, such systems can also be run on dynamic DC connecting voltage. Lower voltage DC Touch minimizes power loss. However, this will also cause substantial fluctuations in grid side converters and higher thermal variations. It is necessary to avoid the protection of the utility grid inverter against highly distorted AC signals, particularly at low switching frequencies. Thermal Simulation of PECs in Solar Power Applications Monitoring DC contact current and voltage ripple analysis, or the method of implementing minimally optimal current regulation, may have two choices to protect the generator side converter from these worse scenarios. However, operating at a constant switching frequency, depending on the grid's power requirements, can lead to higher switching losses due to higher grid-side injection, if the DC connection voltage is not sufficient [16].

2.9 Chapter Summary.

In this chapter, we are introduced to the concept of heat contribution to failure to IGBTs. We then look into the thermal impendence theory, which is used when studying the thermal response of the IGBTs. Concept of the Lab-based cycling tests for lifecycle analysis is introduced. It then looks into the lifetime models used when determining the lifecycle of IGBTs .then it looks at FEM of a single chip IGBT to look into its behaviour with and without air environment. The chapter finalizes by looking at wind and solar technologies reliability.

CHAPTER 3

ACOUSTICS MODELING

3.1 Acoustic Emission

When transient energy waves are produced from a located source in the material by quick energy release, it is referred to as acoustic emission[25]. Acoustic emissions are a defined term in the community of condition monitoring[60]. As a condition control tool for different machines, such as pumps and industrial drives, the acoustic emission is used. In power, semiconductor modules acoustic emissions are an unstudied field not only in terms of condition regulation but as a whole phenomenon.

Acoustic emission is a phenomenon occurring during a power semiconductor switching investigation. Acoustic microscopy was historically used to analyze the evolution of defects in the power semiconductor module and on packaging analysis. The inspection instrument produces acoustic waves and analyzes the returning waves in acoustic microscopy. It's just recently T. J. Karkkainen developed an experimental method to assess if the acoustic emissions in the semiconductors particularly IGBTs are present [61].

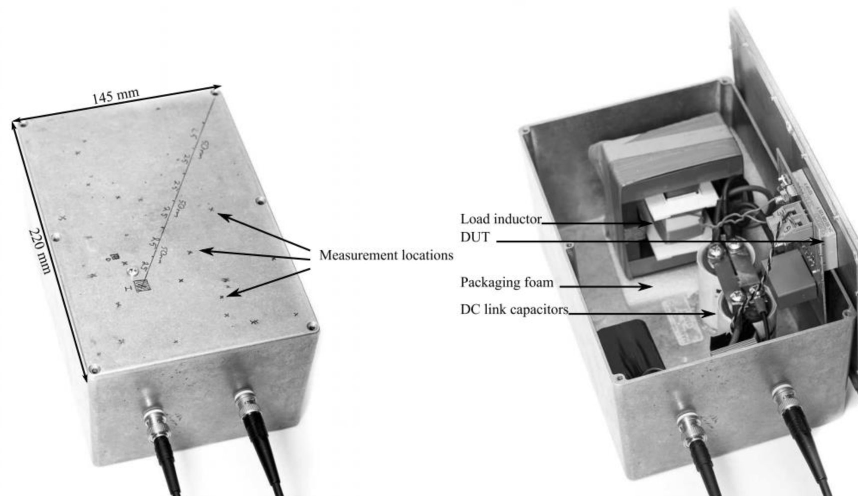

Figure 3.1 Acoustic Measurement Experimental Setup

Experiment findings showed that there is acoustic emission with the action of power semiconductors switching. The strong di / dt induces magnetic activity within the module structure with fast switching to tens of nanoseconds in the tube, and strong currents switched on. [62]. This interaction may cause a force which may be the source of the acoustic emission observed [15].

3.1.1 Acoustic Emission Types

In the experiment, three forms of acoustic emissions were identified, i.e. post-failure emission, immediate emission and switching emission. Comparing the three types of recorded acoustic emissions (Figure 17), it is clear that they vary significantly from each other[63].

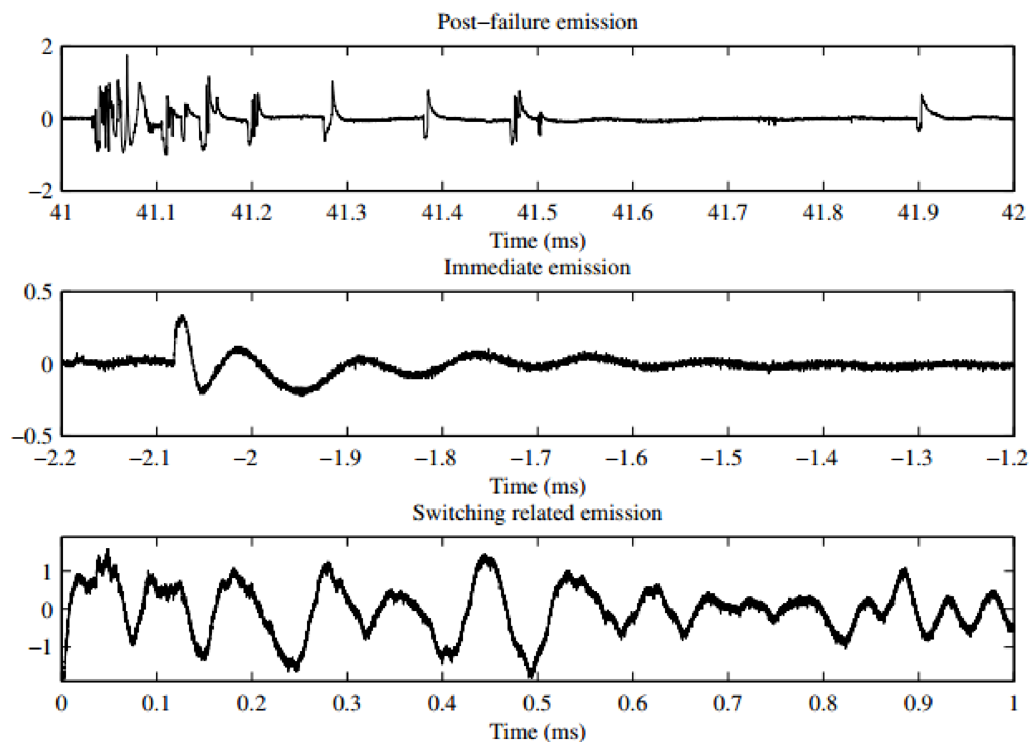

Figure 3.2 Three Types of Recorded Acoustic Emissions

For example, emissions of different durations; the emissions from the malfunction are marginally lower than the acoustic emissions from the switching. After-failure emissions

seem to be a collection of very short "mini-emissions," while direct emissions are more like one oscillation. The switching emission is still a decreasing oscillation, but much longer than the direct emission. But generalization of this quality is risky because the emissions associated with switching and failure from various IGBT modules and experimental configurations have been estimated. The direct emission and switch-related emissions have much in common with waveform and frequency material. All appears to be regulated at a single frequency at 10 kHz. Several other frequencies seem to emit the emission-related switch. By contrast, post-failure emission consists of non-periodically repeated impulse-like signals. The majority of the signal-energy emissions associated with the switch are in the low sub-200 kHz range. The emission period is immediately shorter than that of the corresponding turn. The spectrograms also display the difference in acoustic post-failure emissions from other emission sources: the signal is not one but a series of small broadband events.

Reference acoustics related to switching was calculated at a contact voltage of 600 V DC to decide if the phenomenon is different if transmission of voltage causes it. Three differences are evident when contrasting waveforms (Figure 3.3). First, the signal amplitude was not substantially higher when measuring 600 Volts than when measuring 30 Volts. This means that the phenomenon is more dependent on current than voltage. Thirdly, the condition in terms of acoustics was much shorter. At this point, the explanation for this is unclear. Thirdly, the power module transition induces a slightly higher voltage peak. The sensitivity of the sensor exposes it to interference, and increased voltage exacerbates the interference effect.

It is also evident that the measurement of 600 V created more noise than the measurement of 30 Volts. It is based on small frequency bands, spaced up to 100 kHz apart, starting at around 200 kHz instead of white noise. And if the sensor is removed manually from the experimental device, the noise is shown. While this was not proven, the voltage supply was probably the cause of the noise. Luckily, the acoustic signal is centred below 200 kHz frequencies, and the acoustic signal does not decrease. The signal can be seen in the spectrograms that the 600-volt test broadcast over a more comprehensive frequency range. The low frequencies represent much of the signal power for both experiments. The acoustic event begins with frequencies between 30 and60 kHz at about 0,4 ms in the 600-volt test. Low frequencies are visible at about 0,5 ms in duration. In the 30V trial, the signal is slightly lower at higher frequencies, and the low-frequency signal seems to begin more evenly. Just

at the signal peaks appear fewer frequencies. High frequencies within the range of 600 Volts are distinguished from low frequencies.

Who decides the signals, so it's not clear? The increased voltage, as noted above, did not increase the signal amplitude detected. This suggests that the primary acoustic emission system applies to more magnetic fields and currents than the voltages and electric fields. Another voltage-dependent device can activate other acoustic events that cause the above differences. Partial discharges in silicone gel within the power module are a possible voltage-related mechanism. The test amplitude on the emissions from the switching was very reliable and reproducible. Nonetheless, as can be seen from Figure 3.3, the emissions associated with failure show a very variable magnitude. And it's unclear how relevant such a study is. The emissions associated with switching and failure were measured from various laboratory settings and with specific electrical charges, thereby ensuring that the measuring conditions are not comparable. Nonetheless, it should be noted that each acoustic event is powerful enough for the sensor to capture it, indicating that the choice of sensors was fair [61].

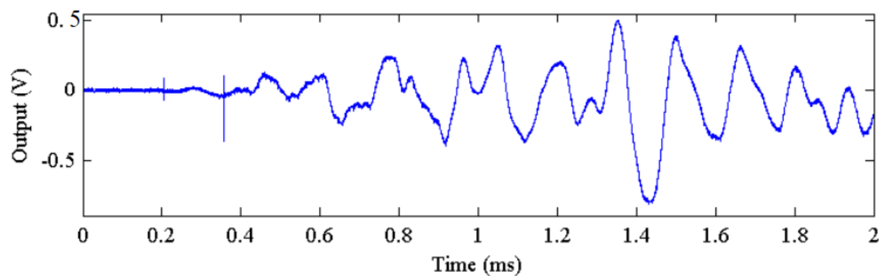

(a) Measurement at 30 V

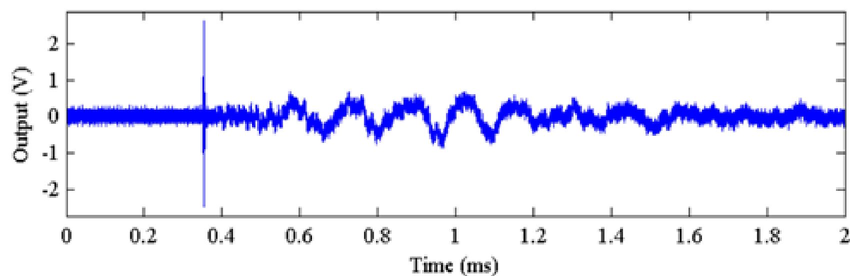

(b) Measurement at 600 V

Figure 3.3 Acoustic Signals

3.1.2 Sensors

There have been two broadband sensors used in the experimental setup, i.e. Kistler Piezotron and KRNBB-PC systems were used. Both sensors ranged from 50 to 400 kHz and from 100 to 100 kHz, respectively. However, the KRN sensor is sensitive to considerably lower frequencies within 10 kHz; the datasheet size is limited to 100 kHz because of the manufacturer's test rig constraints. Both sensors are limited to 60 C; sensor limitation has been circumvented by measuring devices that do not adhere to actual current, power and temperature operating conditions. The author also acknowledged that after the experiments, sensors with temperature ranges up to 160 ° C were available [64].

Figure 3.4 Examples of Sensors for the Wide-Band Acoustic Emission. Two KRNBB-PC Sensors on the Left and One Kistler Piezotron Sensor on the Right

3.1.2 Measurement Challenges and Sensor Performance

The most prohibitive constraint was the temperature range of wide-band sensors that were used. Over a maximum of 60 C, checking where the semiconductors are to be in an area that fits their normal operating area can not be carried out. Use a heat-shielding gel may be able to solve this limitation, but the experience with these gels has not been promising to date.

More sensor issues included the ability to self-resonate. For studies where precise detection of an acoustic effect is an appropriate outcome, it does not pose a problem. Yet although the acoustic phenomena must be accurately recorded, this propensity makes all studies highly contentious. Self-resonance can mask some of the signal characteristics, or at least make determining which elements are real and which are the resulting anomalies inside the sensor more difficult. Nonetheless, the resonance does not seem to exceed the calculation [60].

3.2 COMSOL Simulation

COMSOL's Pressure Acoustics, Frequency Domain (acpr) user interface is used to evaluate IGBT chip acoustics with equations, boundary conditions, and acoustic modelling, sound pressure resolution. The interface is designed to analyze various types of acoustic pressure domain problems, all of which relate to fluid pressure waves. The acoustic model may be part of a broader multi-physical model that defines, for example, the structure-to-acoustic interaction of waves. Pressure Acoustics, Frequency Domain is ideal for modelling acoustic phenomena that do not require fluid flow. For pressure acoustics, the sound pressure p that is recorded reflects the acoustic variances (or excess pressure) of the ambient noise. In the absence of wind, the ambient pressure is the absolute static pressure.

The total acoustic pressure p_t is the estimation of the pressure resolved by the background pressure wave in the presence of the background acoustic pressure wave p_b. For the so-called scattered field formulation, the corresponding equations are formulated using the total strain. Thus, the equations contain background pressure information that could be, for example, a user-defined incident wave or a plane wave. If the geometric dimensions of the acoustic issues are reduced from 3D to 2D or 1D axisymmetrical, the out-of-plane wave number, k_z, and circumferential wave number m may be defined, as applicable. The wavenumber used in k_{eq} equations contains, where appropriate, both the ordinary wavenumber kas and the out-of-plane wavenumber and the circumferential wavenumber. The Pressure Acoustics interface, in the form of background pressure fields and symmetries, solves the entire acoustic problem, including a priori knowledge of the acoustic problem[65].

3.2.1. Sound Pressure Level

Sound pressure can be measured in terms of the datum pressure conforming to the lowermost sound pressure that can be detected by the normal young ear. The result is called the level of sound pressure with decibel units (dB). That is the sum a sound level meter calculates. The sound pressure is a recorded value of the mean root square (r.m.s.) and the p_{ref}= 2 x 10-5 N.m-2 or 20 μPa reference pressure is accepted globally[66]. The equation 11 determines the sound pressure level with the reference pressure taken into consideration:

$$L_P = 20\log_{10} P_{rms} + 94 \quad (11)$$

Pressure, p is in Pascals.

3.2.2 Acoustics of Single Chip Model

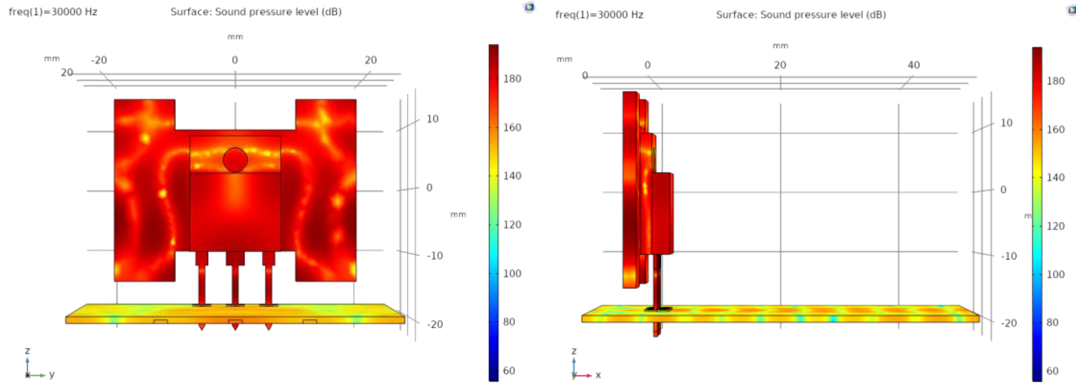

Figure 3.5 Sound Pressure Level Distribution at 30,000Hz

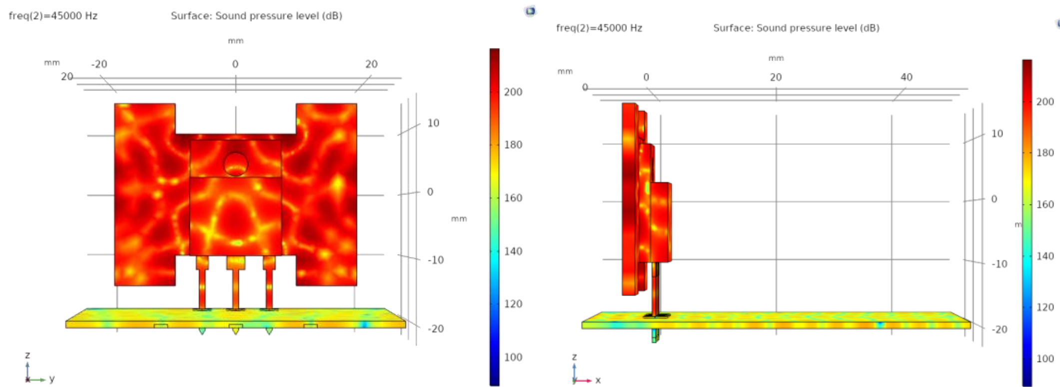

Figure 3.6 Sound Pressure Level Distribution at 45,000Hz

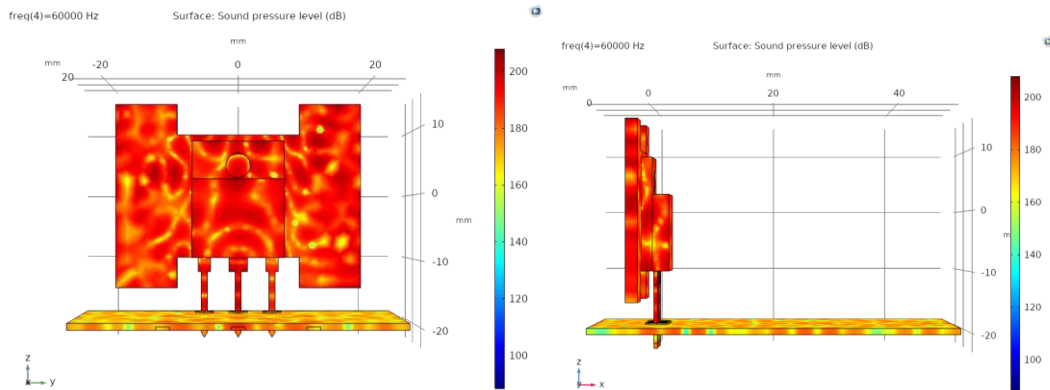

Figure 3.7 Sound Pressure Level Distribution at 60,000Hz

In the first instance simulation was done on the IGBT chip itself and in the second Using COMSOL multiphysics pressure acoustics branch. Similar behaviour was observed as what was observed in the lab setup. The Simulation was run from 30kHz to 60kHz similar frequencies as what was observed in the experimental setup where the acoustic emission was recorded, as shown in figure 3.8. Acoustic emission was observed at 30kHz then declined then peaked at around 50kHz then dropped towards 60kHz, thereby verifying the different types of acoustic emissions as described in the lab experiment.

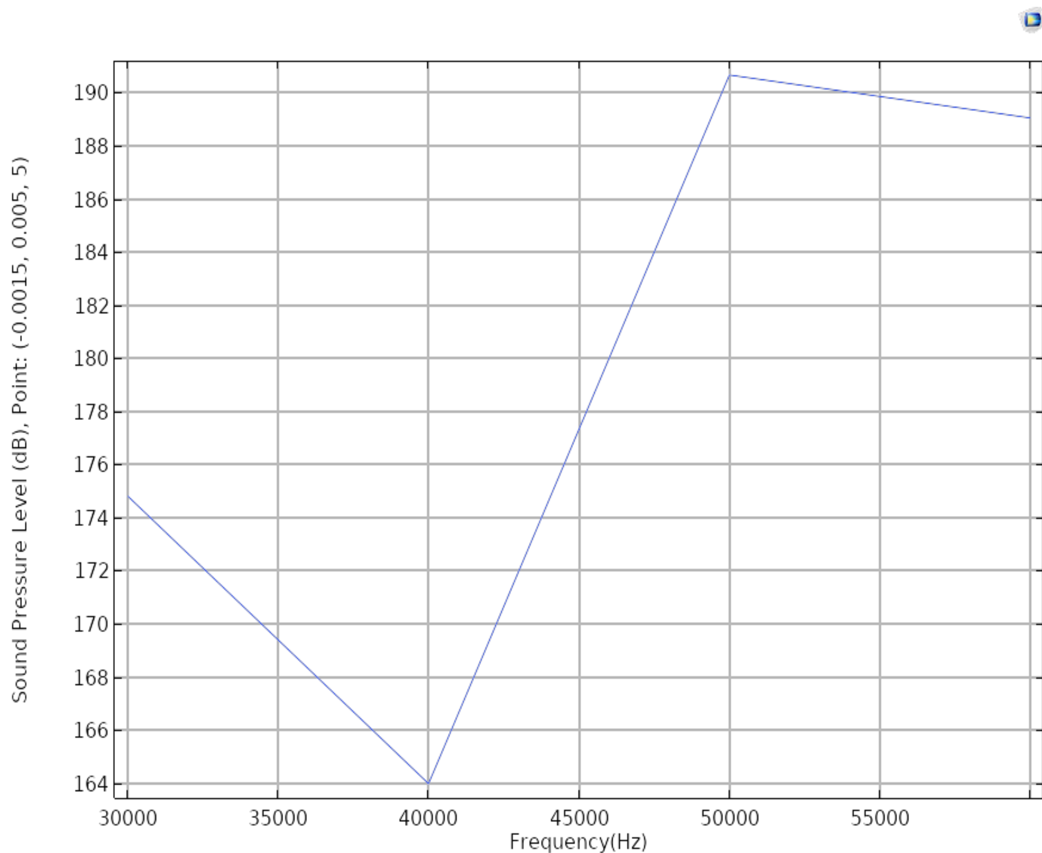

Figure 3.8 Graph of Sound Pressure Level against Frequency

3.2.3 Acoustics of Single Chip Model in Surrounding Air

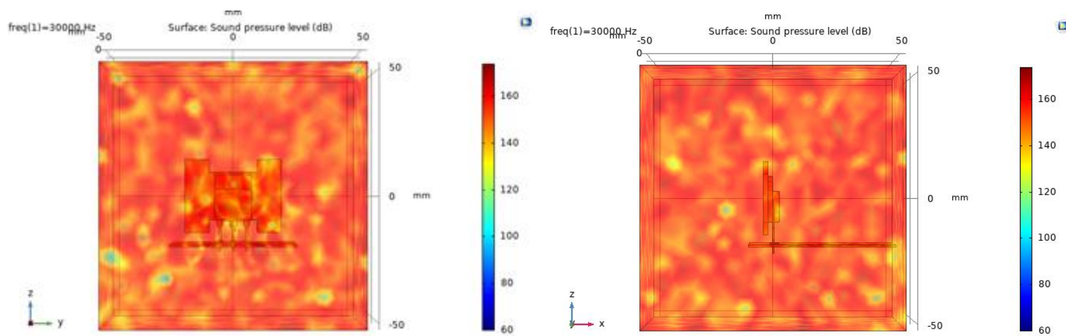

Figure 3.9 Sound Pressure Level Distribution at 30,000Hz

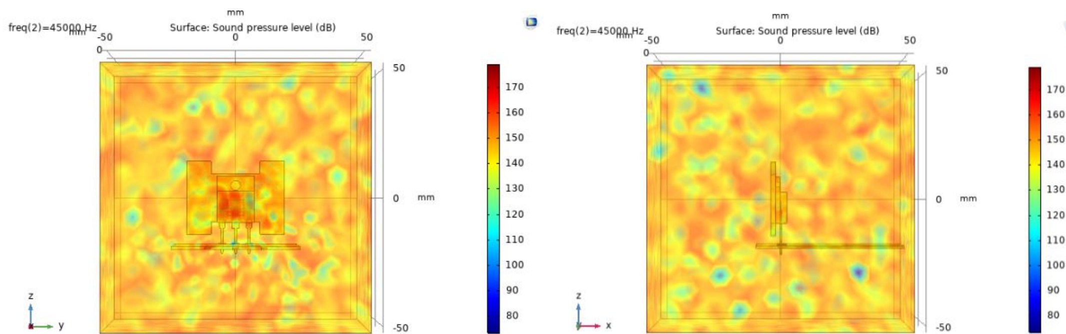

Figure 3.10 Sound Pressure Level Distribution at 45,000Hz

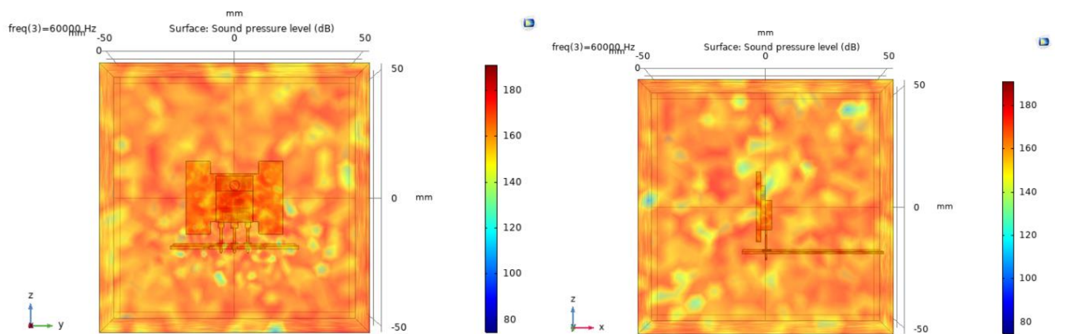

Figure 3.11 Sound Pressure Level Distribution at 60,000Hz

In the second instance, Simulation was done on the IGBT chip surrounded by a block of air Using COMSOL multiphysics pressure acoustics branch. Similar behaviour was observed as

what was observed in the lab setup. The Simulation was run from 30kHz to 60kHz similar frequencies as what was observed in the experimental setup where the acoustic emission was recorded, as shown in figure 3.12. The surrounding air seemed to bring out an effect of reducing the amounts of sound pressure levels recorded. Though the behaviour of the acoustic emission remained the same from 30kHz to 50kHz, and a difference was observed from 50kHz to 60kHz.

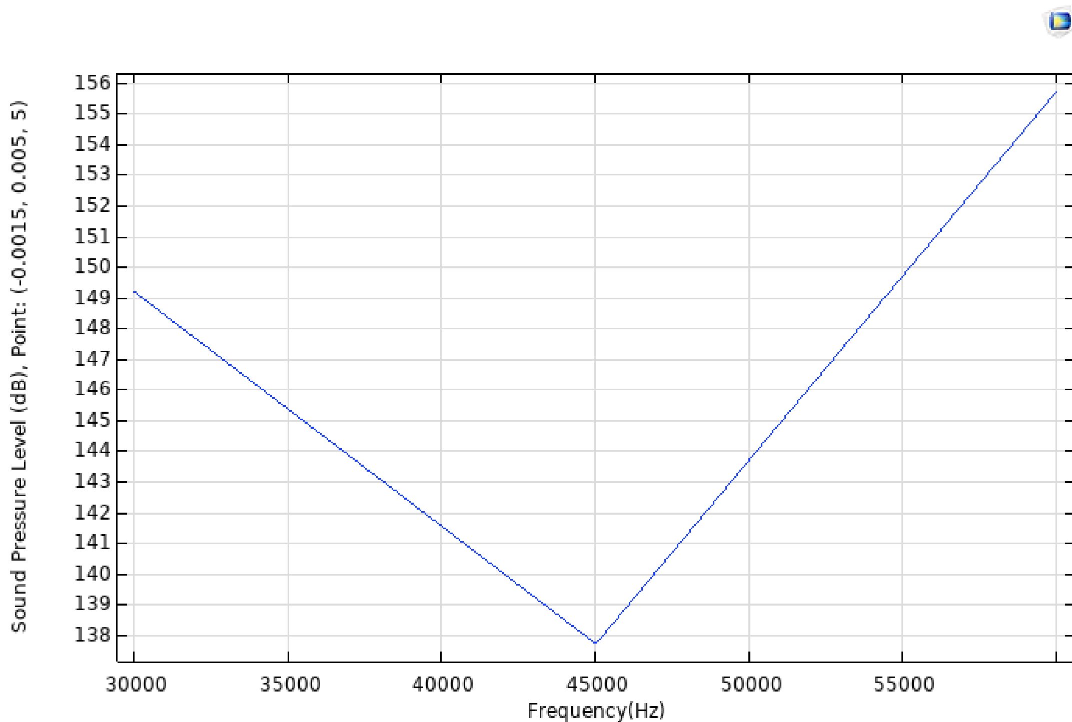

Figure 3.12 A Graph of Sound Pressure Level against Frequency

3.2 Chapter Summary.

In this chapter, we look into the experimental study which verified the existence of acoustic emissions in IGBTs using various sensors. The chapter looks at the three different acoustic emissions observed using the mentioned sensors. The chapter also using the experimental data incorporates the data into COMSOL Multiphysics to determine the legitimacy of the data, which is verified by figure 3.12 produced from the simulation.

CHAPTER 4

SIMULATION MODELLING RESULTS AND DISCUSSION

The chapter's primary purpose is to present the findings of the thesis work and to analyze the results. It is divided into three main chapters' subchapters. Firstly, the results from the COMSOL results using thermoviscous physics. Secondly, lifetime analysis of the results obtained from COMSOL using EXCEL by relating the data using existing lifetime models.

The first goal of this study is first to evaluate the relationship between heat and acoustics. The second goal of the study is to investigate the effect of both on the Reliability of the IGBTs. Purpose, this chapter sets out the formulas for both domains. The heat-acoustics relationships are assessed using COMSOL software, and Reliability is accessed using EXCEL by incorporating existing lifetime models.

Many complex factors must be taken into account when modelling acoustic phenomena, particularly in small geometric devices. The Thermoviscous Acoustics Interface gives an easy and accurate way to set up and solve the acoustics model for conditions such as acoustic pressure and temperature variance[67].

Thermoviscous Acoustics interface (ta) Under the Thermoviscous Acoustics branch is used to measure the acoustic variance of sound, speed and Temperature by incorporating a physics interface. This interface of physics is necessary to accurately model acoustics in small geometries. Viscous loss and thermal conduction become necessary near walls because there is a boundary layer. The thicknesses of boundary layers are known as the viscous and thermal penetration depth. Of this purpose, the governing equations will specifically include thermal conduction effects and viscous losses. This is used to model transducers such as microphones, miniature loudspeakers and receivers, for example. Other uses include collecting feedback on hearing aids or receiving the damping movements of MEMS systems. The framework in physics solves equations which are harmonic in all fields and sources within the frequency domain.

The equations defined by the Thermoviscous Acoustics, Frequency Domain interface are linearized Navier-Stokes equations that solve the continuity, momentum, and energy equations under quiescent background conditions. The model simultaneously solves

acoustic pressure p, acoustic velocity u variance (particle velocity), and acoustic temperature variances, T, due to the rigorous definition needed to model Thermoviscous acoustics [68].

The Thermoviscous Acoustics, Frequency Domain interface, solves the length scale at which the thermoviscous acoustic definition is provided by the thickness of the viscous boundary layer for the propagation of compressible linear waves into a general viscous and thermally conductive fluid, which is

$$\delta_v = \sqrt{\frac{\mu}{\pi f \rho_0}} \tag{4.1}$$

and the thickness (thermal penetration depth) of the thermal boundary layer is

$$\delta_v = \sqrt{\frac{k}{\pi f C_p}} \tag{4.2}$$

Frequency = f.

Dynamic viscosity= μ.

Equilibrium pressure= $\rho_{0.}$

Thermal conductivity = k.

Heat capacity at constant Pressure = C_p.

The thickness of the two boundary layers depends on the frequency f and decreases as frequency increases. The two-length scales have to do with the nondimensional Prandtl number Pr, by

$$\frac{\delta_v}{\delta_t} = \sqrt{\frac{\mu C_p}{k}} = \sqrt{Pr} \tag{4.3}$$

That defines the relative importance for a given material of thermal and viscous effects. At a thickness of 0.22 mm at 100 Hz in the air with 20 C and 1 atm, while at the water under similar conditions, there is just 55µm of thickness. The number of Prandtl in the air is 0.7, and in water, it is 7[69].

In the research Using COMSOL Multi-physics software, a single IGBT chip was designed in the software and was used to establish a relationship between acoustics and the heat module. The model is based on the actual physical measurements and material properties shown in the table below. Linearized Navier-Stokes equations are defined for the whole model at the sound pressure and frequency levels when the input heat is applied. The meshed outlook of the model is shown below.

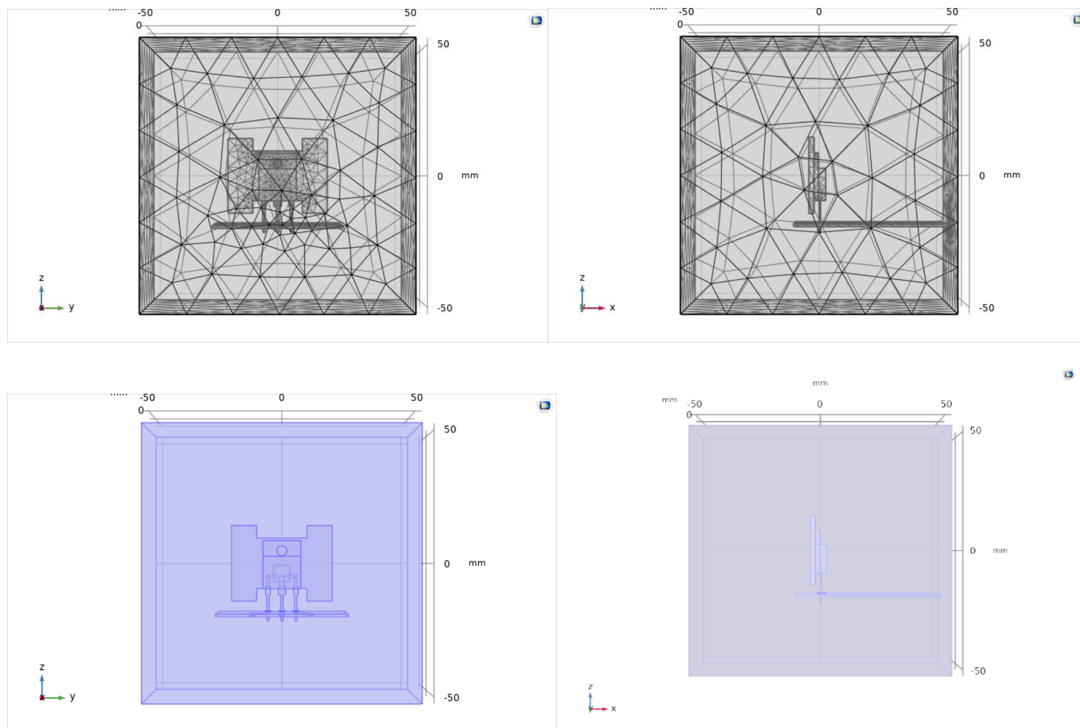

Figure 4.1 Physical View of the Module

Using COMSOL, thermoviscous acoustics physics was applied with a heat source of 75W was used, and acoustic pressure distribution was observed as shown below at 10 kHz, 50 kHz and 100 kHz.

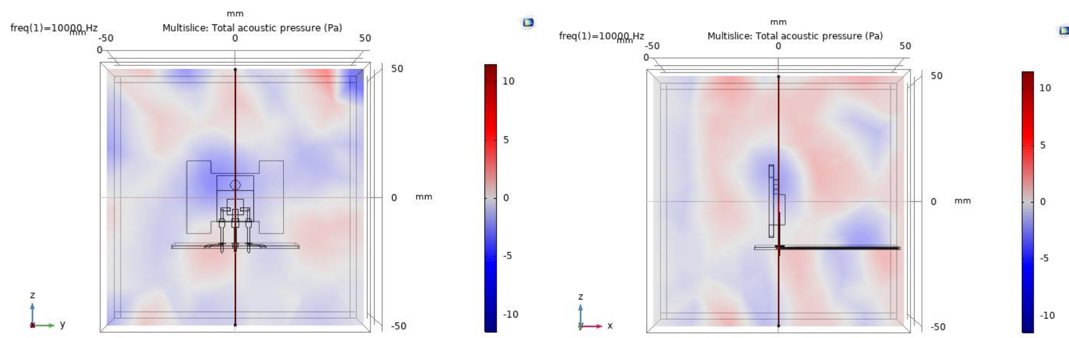

Figure 4.2 Acoustic Pressure Distribution at 10 kHz with A 75W Heat Source

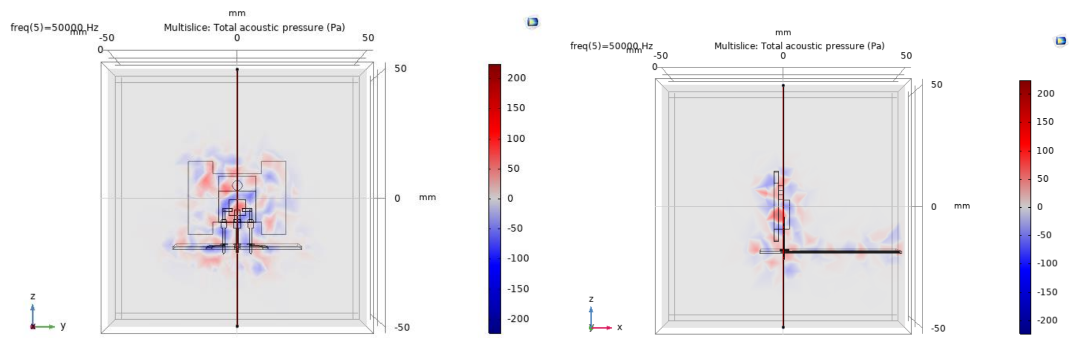

Figure 4.3 Acoustic Pressure Distribution at 50 kHz with A 75W Heat Source

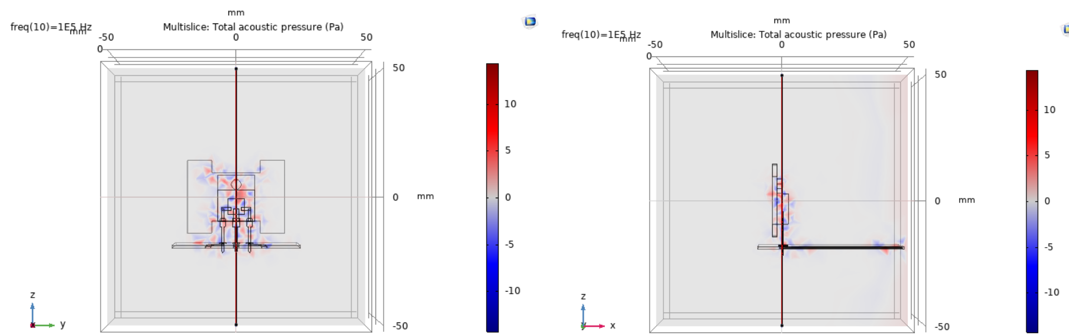

Figure 4.4 Acoustic Pressure Distribution at 100 kHz with A 75W Heat Source

Looking at figures 29,30 and 31 when can see that the sound pressure levels are distributed more evenly on the lower frequencies, and at the higher frequencies, they are concentrated around the chip. After running the model through COMSOL, we obtained data from 10Hz to 100 kHz of Sound pressure level against these frequencies at a constant heat source of 75W, as shown in Appendix A. The Simulation was run severally using different steps to get a varied range of data we then used curve fitting technique using Microsoft EXCEL software to get equations that define the Frequency and acoustic pressure level at 75W.

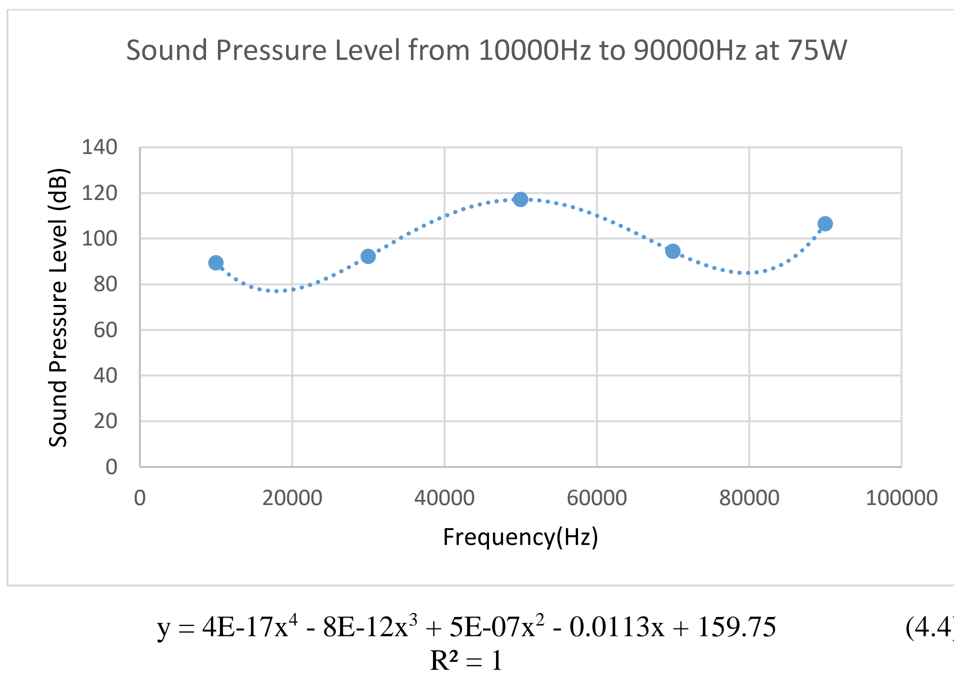

$$y = 4E\text{-}17x^4 - 8E\text{-}12x^3 + 5E\text{-}07x^2 - 0.0113x + 159.75 \quad (4.4)$$
$$R^2 = 1$$

Figure 4.5 Sound Pressure Level from 10000Hz to 90000Hz at 75W

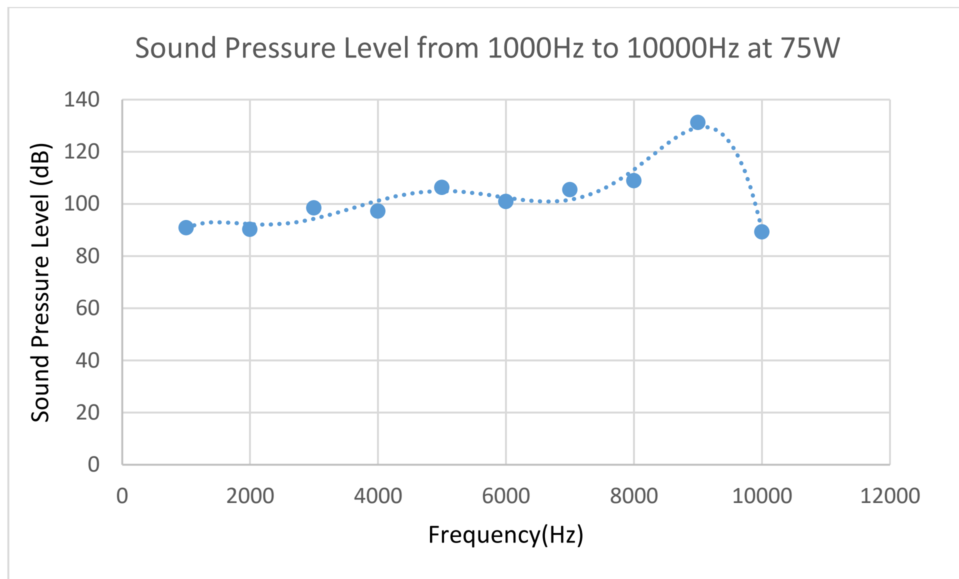

$$y = -2E\text{-}20x^6 + 5E\text{-}16x^5 - 6E\text{-}12x^4 + 3E\text{-}08x^3 - 9E\text{-}05x^2 + 0.1113x + 39.88 \quad (4.5)$$

$$R^2 = 0.9434$$

Figure 4.6 Sound Pressure Level from 1000Hz to 10000Hz at 75W

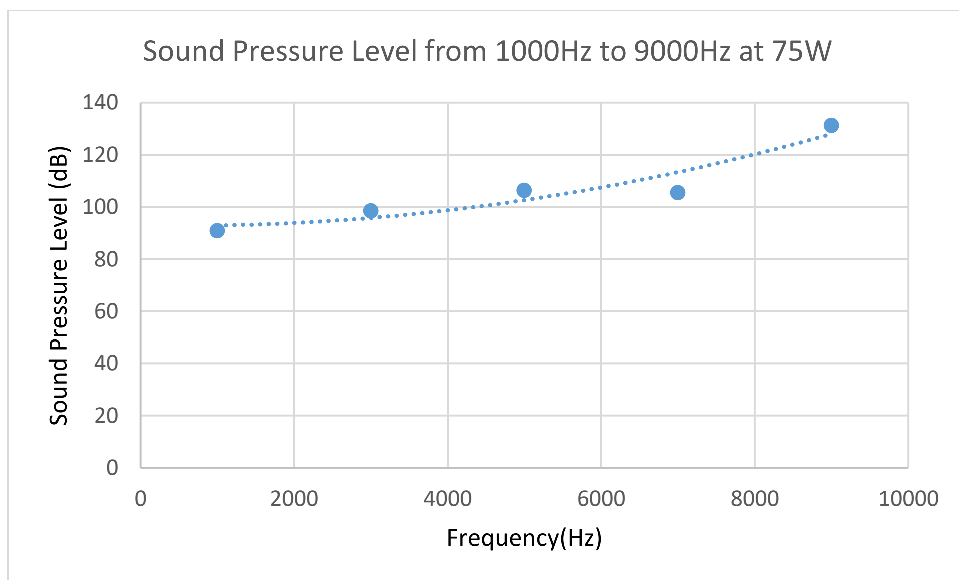

$$y = 5E\text{-}07x^2 - 0.0005x + 92.977 \quad (4.6)$$

$$R^2 = 0.8932$$

Figure 4.7 Sound Pressure Level from 1000Hz to 9000Hz at 75W

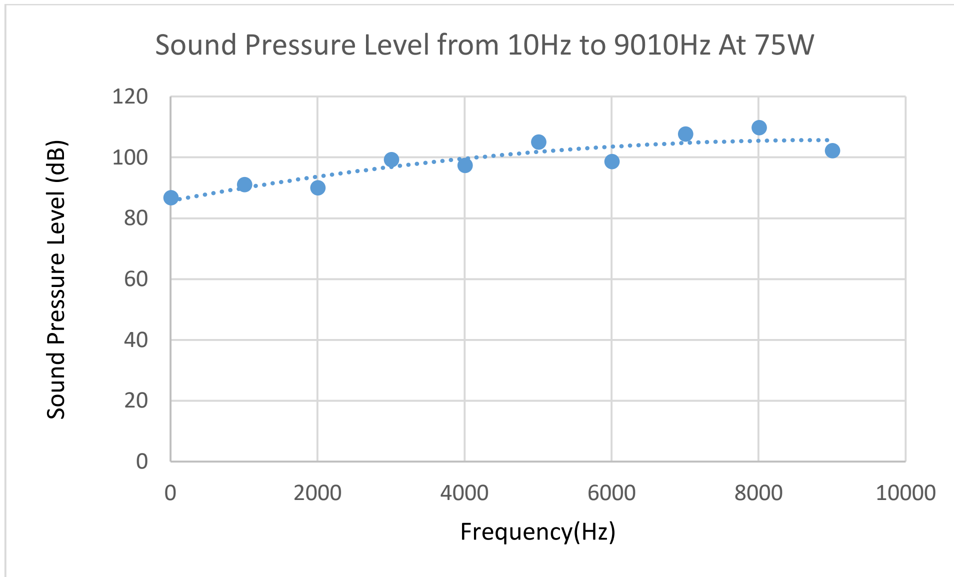

$$y = -2E\text{-}07x^2 + 0.0045x + 85.761 \quad (4.7)$$
$$R^2 = 0.8134$$

Figure 4.8 Sound Pressure Level from 10Hz to 9010Hz at 75W

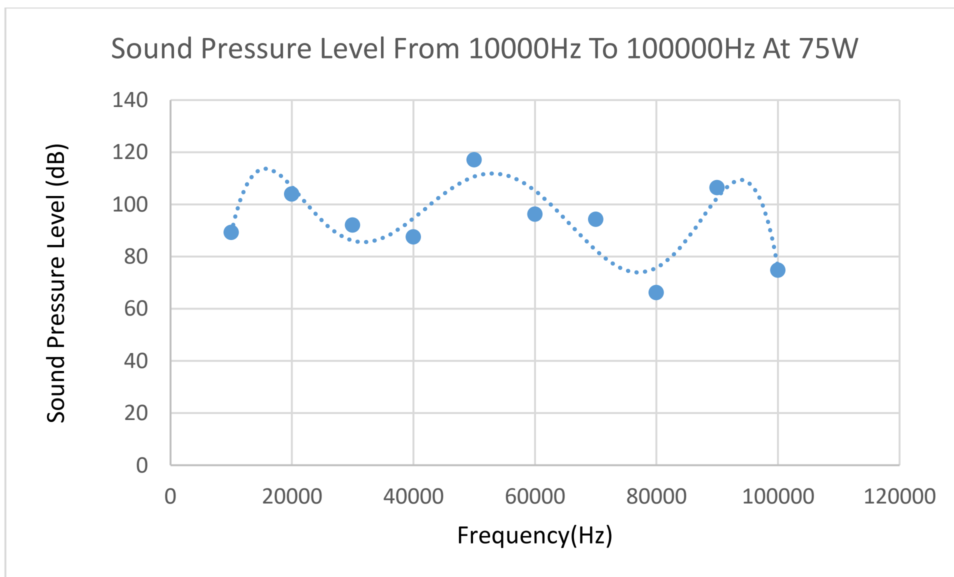

$$y = -6E\text{-}26x^6 + 2E\text{-}20x^5 - 2E\text{-}15x^4 + 2E\text{-}10x^3 - 5E\text{-}06x^2 + 0.0679x - 249.71 \quad (4.8)$$
$$R^2 = 0.7666$$

Figure 4.9 Sound Pressure Level from 10000Hz to 100000Hz at 75W

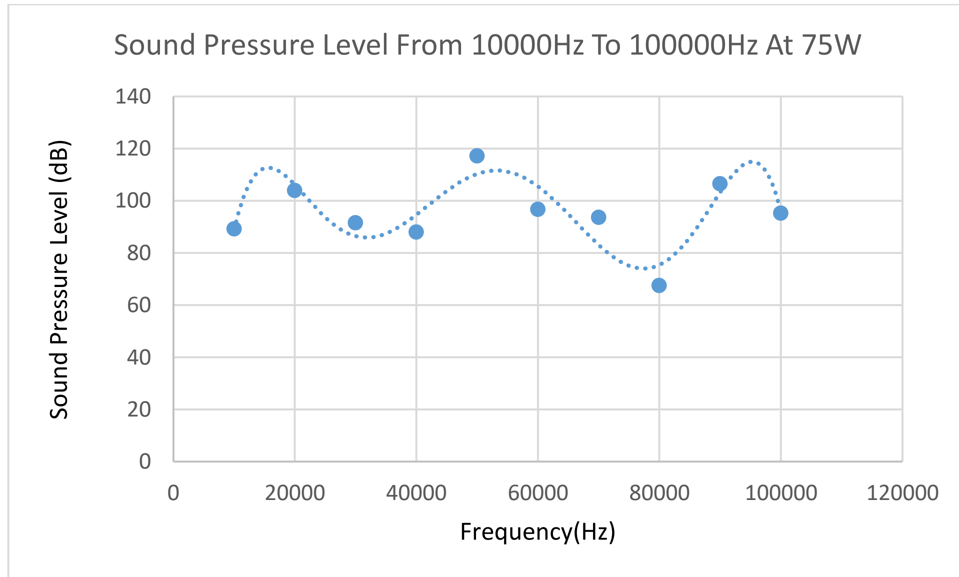

$$y = -5E\text{-}26x^6 + 2E\text{-}20x^5 - 2E\text{-}15x^4 + 1E\text{-}10x^3 - 4E\text{-}06x^2 + 0.0644x - 233.3 \quad (4.9)$$

$$R^2 = 0.7542$$

Figure 4.10 Sound Pressure Level from 10000Hz to 100000Hz at 75W

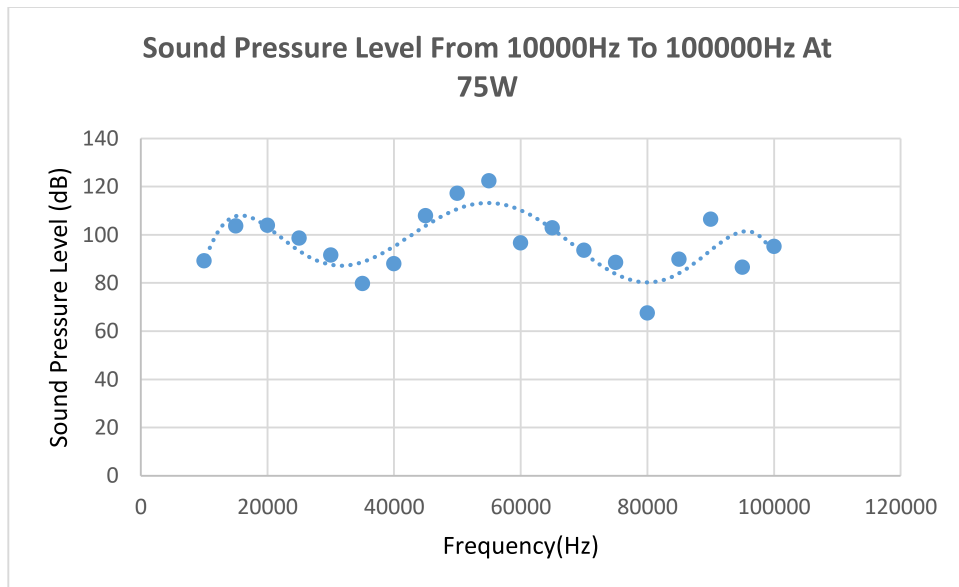

$$y = -4E\text{-}26x^6 + 1E\text{-}20x^5 - 2E\text{-}15x^4 + 1E\text{-}10x^3 - 4E\text{-}06x^2 + 0.0517x - 172.31 \quad (4.10)$$

$$R^2 = 0.614$$

Figure 4.11 Sound Pressure Level from 10000Hz to 100000Hz at 75W

Considering the above figures looking at the equations and R values obtained, it was determined that the fewer the number of steps, the better the R-value and vice Versa. In the Figure 4.12 of Frequency against sound pressure level, we can see the sound pressure level peaked around 50 kHz declined then subsequently had a smaller peak at about 90 kHz.

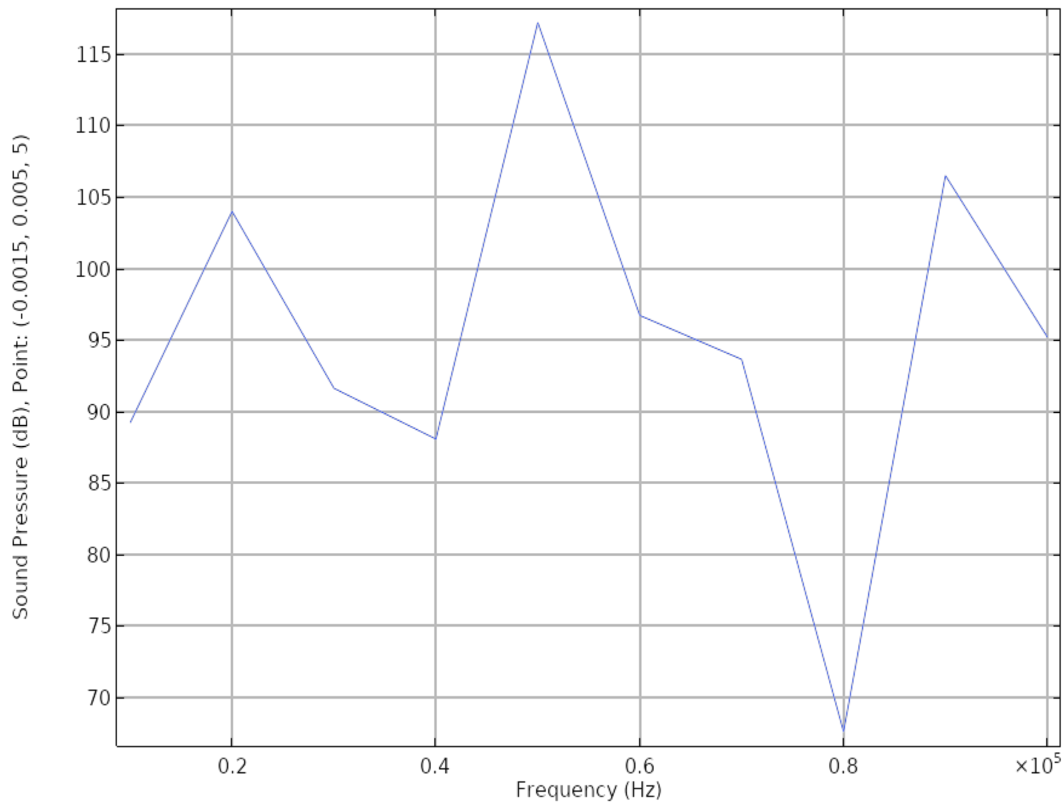

Figure 4.12 Sound pressure (dB) against Frequency

Since for thermoviscous physics in COMSOL Multiphysics utilizes only heat source sub-physics Using the joule heating physics we determined different values of heat at different temperatures and were able to come up with a relationship between the two as shown by figure 40 and equation 18. The relationship itself is linear.

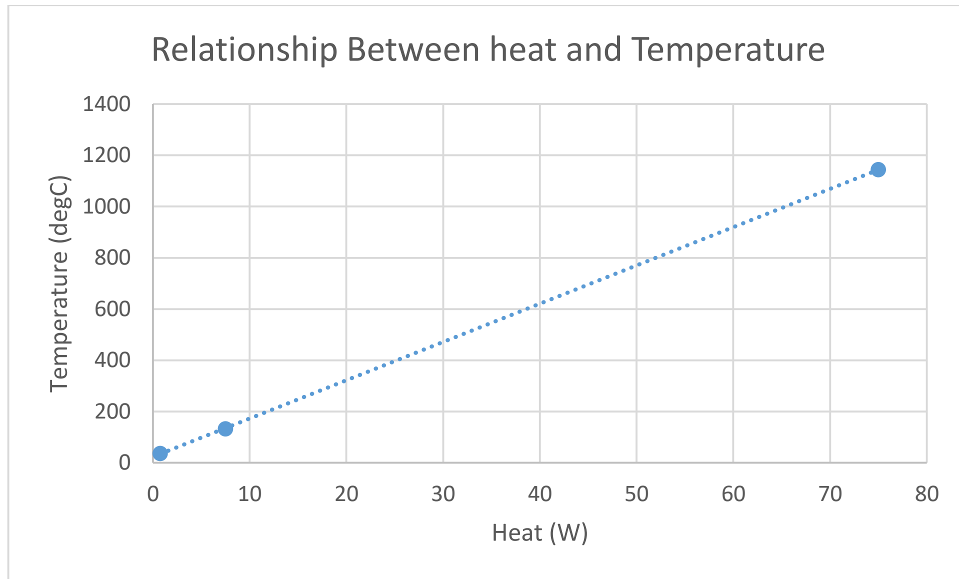

$$y = 14.945x + 22.944 \qquad (4.11)$$

$$R^2 = 1$$

Figure 4.13 Relationship between Heat and Temperature

Using thermoviscous Multiphysics, we simulated for the sound pressure levels at 30 kHz while giving the Specimen three different heat source levels, i.e. 0.75W, 7.5W, 750 Wand 7500W. Using these results, we were able to come up with a relationship between heat and sound pressure levels which was linear.

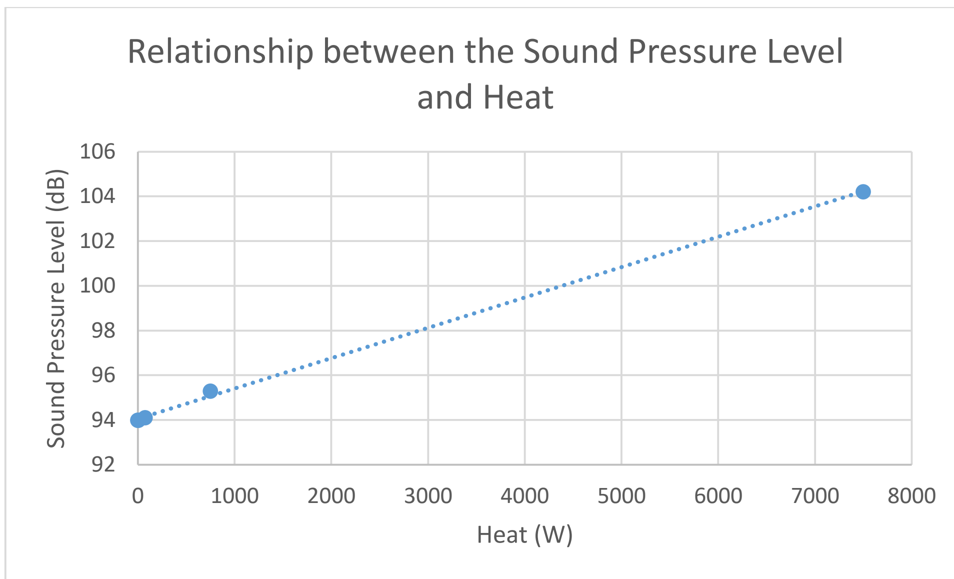

$$y = 0.0014x + 94.057 \tag{4.12}$$

$$R^2 = 0.9992$$

Figure 4.14 Relationship between the Sound Pressure Level and Heat

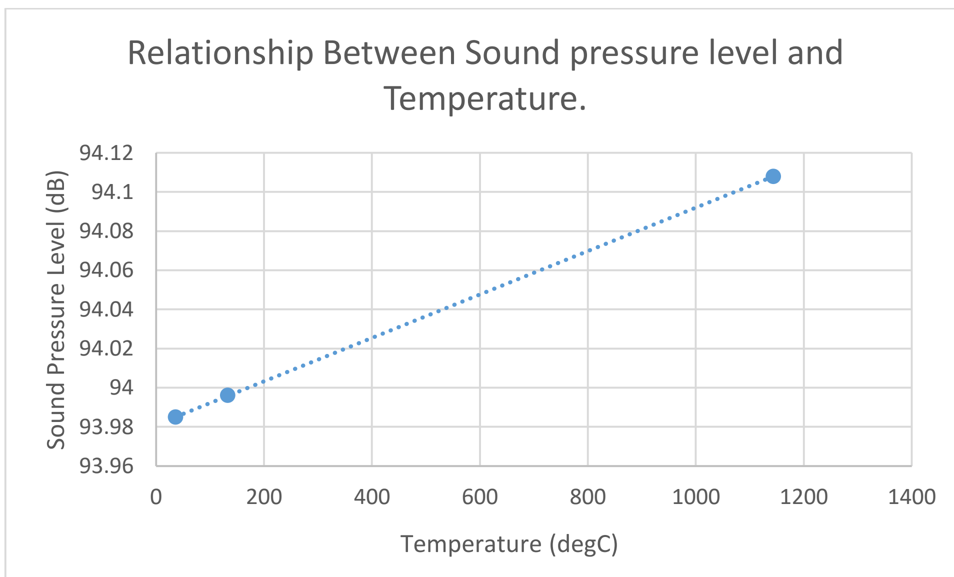

$$y = 0.0001x + 93.981 \tag{4.13}$$

$$R^2 = 1$$

Figure 4.15 Relationship between Sound Pressure Level and Temperature

Conversely using the relationship between Temperature and heat, we were able to get a relationship between Sound pressure level and heat generated.

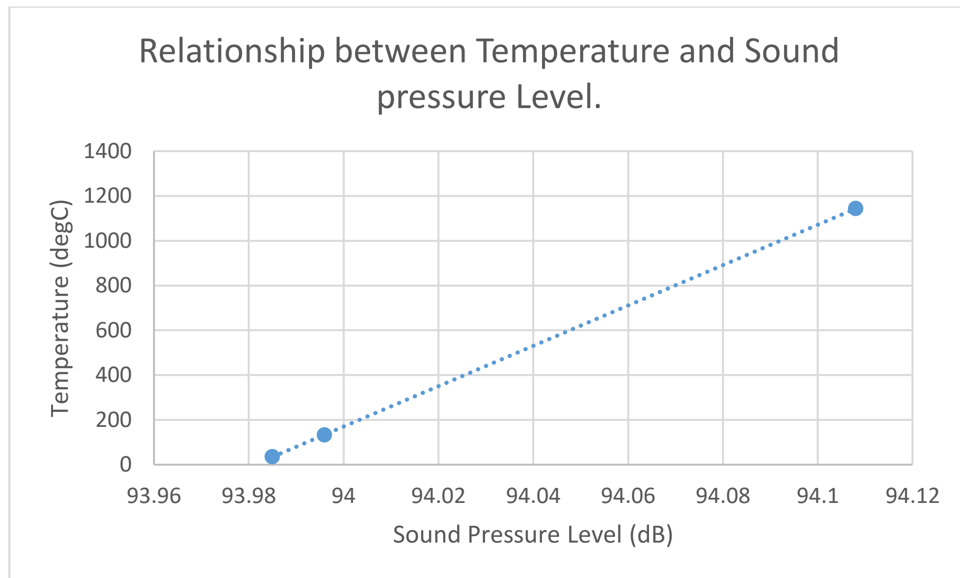

$$y = 9015.7x - 847308 \qquad (4.14)$$

$$R^2 = 1$$

Figure 4.16 Relationship between Sound Pressure Level and Temperature

4.1 Reliability Modeling and Lifetime Analysis

Reliability modelling for IGBTs is given in this section. The measurement of PEC lifetime projections, electro-thermal, and thermo-mechanical and thermal models developed using COMSOL Multiphysics, is extended further. Weibull figures analyze lifetime study for electronic control devices. Data from the IGBT model was analyzed to assess the number of failure cycles. PECs are primarily secured by the related switching elements (IGBT), which are the most easily damaged components [70]. The failure occurs mainly because of the heat-mechanical stress caused during temperature changes by various thermal expansion characteristics of materials within the IGBT. The failure mechanisms of these instruments

are connected to the cycling load of the assembly. Therefore, the IGBT temperature profile was considered in terms of mean and cyclic temperature to predict the lifetime [16].

Analytical performance models are built in relation to failure mechanisms and quantified reliability to predict lifetime such as:

Coffin–Manson Model:

$$N_f = \alpha\ (\Delta T_j)^{-n} \qquad (4.15)$$

Whereby ΔT_j is the junction temperature fluctuation and α and n are constants, obtained experimentally.

Coffin–Manson–Arrhenius Model:

$$N_f = A(\Delta T_j)^{\alpha} \cdot e^{(\frac{E_a}{k_b \cdot T_m})} \qquad (4.16)$$

Whereby Tm is the mean junction temperature .k_b is the Boltzmann constant and E_a is activation energy parameter[71].

Norris–Landzberg Model:

$$N_f = A.f^{-n_2}(\Delta T_j)_{\rho}^{-n_1}(\frac{E_a}{k_b \cdot T_m}) \qquad (4.17)$$

(24)

This model goes a step further by including, *f* of the junction temperature, which is the cycling frequency. The model itself is a sort of an enhancement of the Coffin–Manson–Arrhenius Model.

Bayerer Model:

$$N_f = K \cdot (\Delta T_j)^{-\beta 1} \cdot e^{(\frac{\beta_2}{T_m})} \cdot t_{on}^{\beta 3} \cdot I^{\beta 4} \cdot V^{\beta 5} \cdot D^{\beta 6} \qquad (4.18)$$

Whereby t_{on} is the heating time, *I* is the applied DC on the diameter of the bond wire, and V is the blocking voltage.

Palmgren – Miner linear damage accumulation rule can also be used and modelled for failure prediction in order to determine the total life consumption (TLC) that comes as a result of the combined effect load profile. It is expressed as:

$$LC = \sum_{i=1}^{j} \frac{n_i}{N_i} \tag{4.19}$$

Whereas n_i is the number of cycles, N_i is the lifetime calculated in the ith profile, and j is the total load profile. The rule says failure occurs when the condition is met TLC = 1 [72].

4.2 Lifetime Analysis for Discrete IGBT Devices

In this research, we used Step Function in COMSOL Multiphysics to be able to get the number of cycles based on the IGBT model using Joule heating Physics. From the data, we obtained, we were able to get the mean Temperature and temperature variation of the cycles. A modified model for life Coffin – Manson – Arrhenius was then Used whereby Temperature mean, Tm and temperature variation are used to define failure cycle (N_f). N_f Is defined as the number of cycles expected before failure occurs, The Boltzmann constant (k_b) is $1.38 \times 10^{-23} JK^{-1}$, the activation energy $1.3 \times -10^{-19} J$, A and α which are constants 610 and −5 respectively were used in the model to come up with N_f.

Incorporating a step function into our model, the number of cycles could be determined, as shown in figure 44 below.

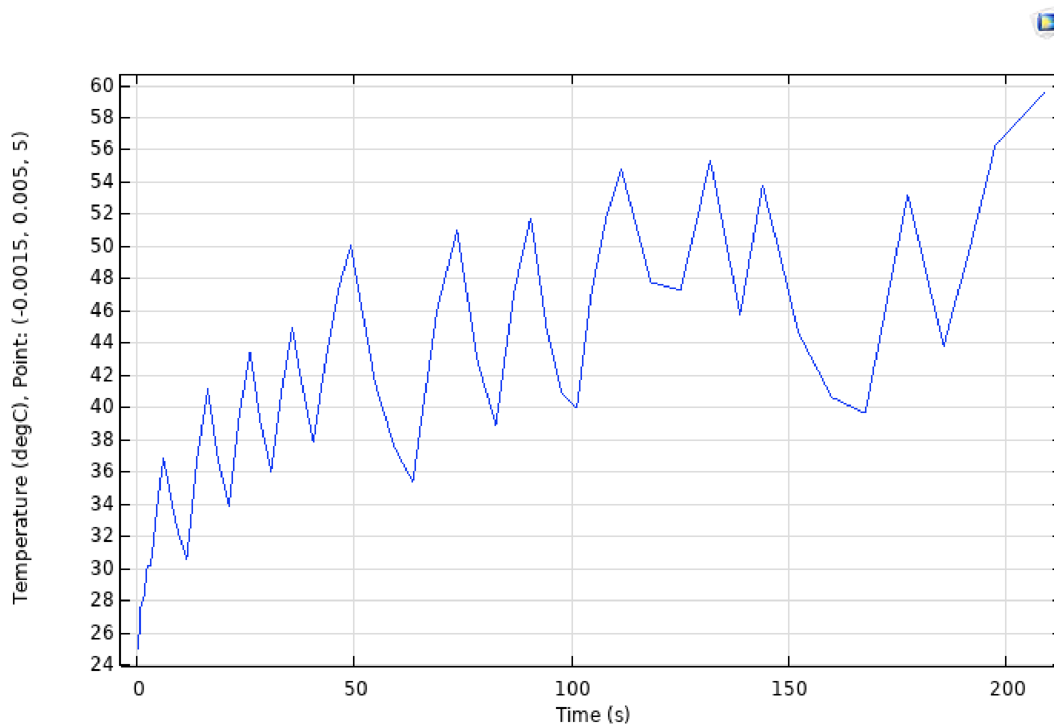

Figure 4.17 Graph of Temperature against Time

Using the above Figure 4.17, we were able to determine the number of respective cycles. Considering the maximum and minimum temperatures between consecutive peaks, we came up with mean temperatures and temperature variations of the Simulation, as shown in the Figure 4.18 and Appendix.

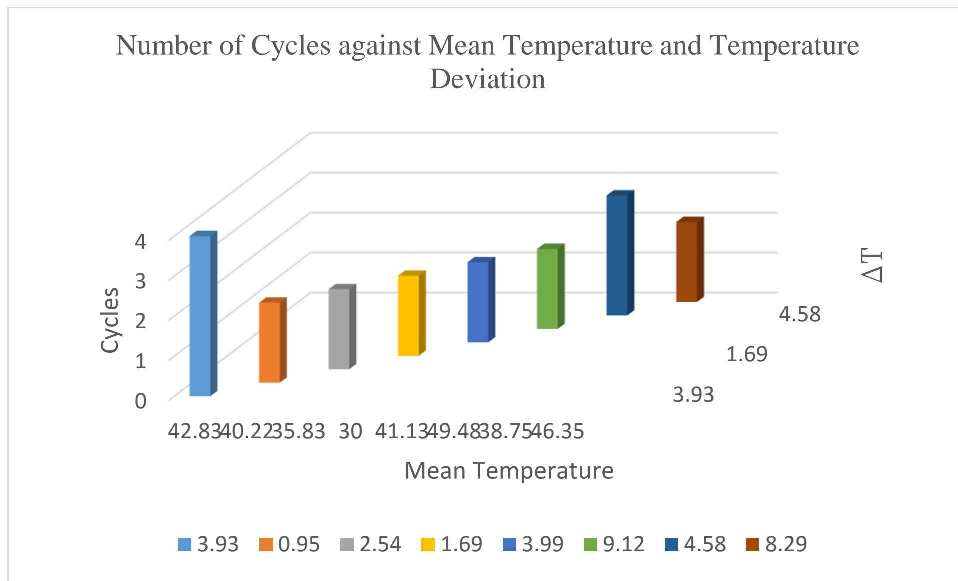

Figure 4.18 Number of Cycles against Mean Temperature and Temperature Deviation

Using the Coffin–Manson–Arrhenius Model described earlier, we were able to get the value of N_f of the cycles we obtained as shown below in Figure 4.19. The values used were the ones obtained from figure 45 and feed into the equation 4.16.

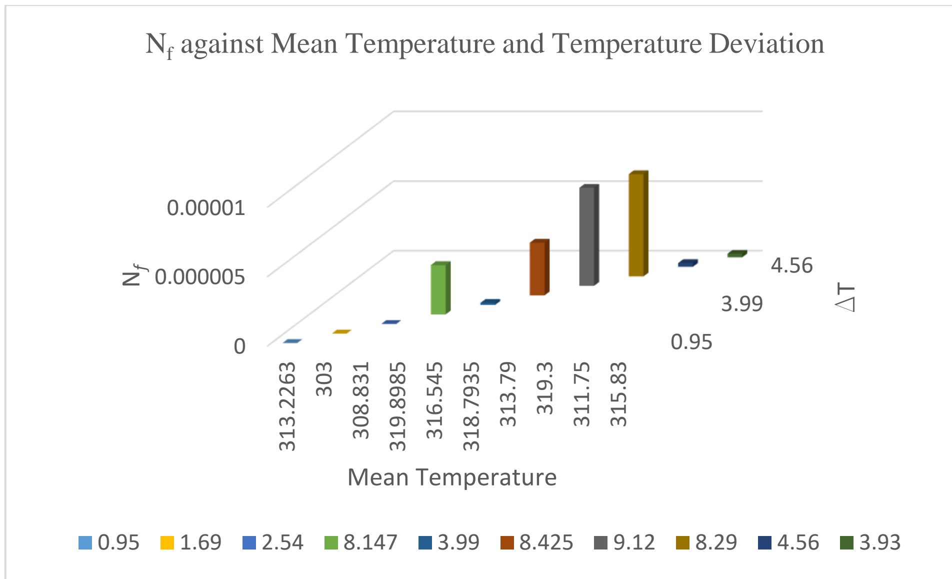

Figure 4.19 N_f against Mean Temperature and Temperature Deviation

Given that we have obtained the value of $N_{f,}$ we will be able to employ the Palmgren – Miner linear damage accumulation rule to determine the lifetime consumption considering TLC= 1 when the failure occurs.

In our case, we did a 200 Seconds simulation and summing up the values of N_f from Table A.8 the value of lifetime consumption we get is 0.000106601 which is still far from failure given that the value has to be 1 when the total failure occurs.

Considering the accuracy of acoustics sensors and the difficulty of determining the lifetime of the IGBTs chips, especially towards the end of life of the chips. Using our developed relation of temperature and acoustics, we can accurately be able to determine the temperatures using acoustics sensors. This will enable us to assess the health of the device better and prevent total failure early in advance by doing preventive measures before the actual failure event happens. This will be more sustainable and economical to the organizations whereby the electronic devices would be used for longer reducing on electronics wastes, and there will be less downtime saving money for the organization.

4.3 Chapter Summary

In this chapter, we look into the modelling of the single IGBT chip surrounded with air by using COMSOL Multiphysics thermoviscous physics to determine the relationship between heat and acoustic measured as sound pressure level. After obtaining the data, we use the curve fitting method using Microsoft EXCEL to formulate equations defining the connection between Frequency and sound pressure level measured in dB as described by equations 12 to 18. Using data obtained from COMSOL by introducing a step function lifetime analysis was carried out by means of the Coffin–Manson–Arrhenius Model.

CHAPTER 5

CONCLUSIONS AND FUTURE WORK

The thesis is concluded by summing up the most critical results discovered in the thesis work. This chapter also details how this thesis dealt with the objectives proposed in Chapter 1. At the end of this chapter are also discussed the possible future study directions and plans as a follow-up to this thesis.

The current emphasis on renewable technologies has made the uptake of power electronic devices to be higher, which increases by the day. Most research was traditionally done on the effect of heat on the electrical conversion devices because most failure rates were linked to the heat produced by the devices. Acoustics phenomena have usually been used in the condition monitoring field to monitor the health of industrial machines. Its is only recently a study was done by T. J. Karkkainen to verify and confirm the existence on these acoustics emissions using sensors in a lab setup which was later verified using an Oscilloscope.

5.1 Summary of Research Findings.

The thesis attempts initially to look into the common failure types found in IGBT chips and look into what commonly causes them. It then precedes by looking into the industry standard of condition monitoring the failure and how it is frequently done in practice. Considering most failure is caused by heat, the thesis provides a comprehensive review on the modelling of heat in the semiconductor devices by looking into the current research being done in lab analysis and modelling using COMSOL Multiphysics. The thesis then introduces the acoustics phenomena research, which is relatively new in the field of power electronics which traditionally has been considered only on condition monitoring. The paper then looks into the research been done on verification on the availability of acoustic emissions using sensors then goes further by verifying the data using COMSOL Multiphysics. Using COMSOL, the thesis now goes into the main study using thermoviscous physics looks into the relationship between heat and acoustic emission and using curve fitting a relationship is determined between the two. This is done using a constant heat source of 75W and running the model with various frequencies to obtain sound pressure levels which, in our case,

represented the acoustic phenomena. Using data obtained from COMSOL by introducing a step function lifetime analysis was carried out by using the Coffin–Manson–Arrhenius Model. The following takes can be considered as the main findings of this research work:

- There is a relationship between heat and Acoustics in IGBT chips as verified by the equations we obtained using curve fitting of the model data.
- The acoustic phenomena behaviour follows an inconsistent profile by peaking at specific frequencies. From our simulations, we can identify three peaks at around 20 kHz. 50 kHz and 90 kHz verifying the observations made by T. J. Karkkainen that there are three types of acoustics emission types as discussed in the acoustics section.

5.2 Scope for Future Research Direction.

The present research work being done has focused on firstly relating heat and acoustics emissions using COMSOL Multiphysics. The data we obtained was used to determine IGBT's lifespan using Coffin–Manson–Arrhenius Model by introducing a step function into the COMSOL model. The following steps can be taken to improve on and continue with our current research:

- This research did modelling on a single IGBT chip on two environments, i.e. with and without surrounding air. For future analysis, it would be great to look into the behaviour of multichip models to determine if it affects the relationship we have established.
- Future work may consider real-world data by carrying out lab analysis using actual IGBT chips to determine to find out if the data corresponds to the simulated data.
- The current research only considers Silicon material on the IGBT chip. In the future, different materials like carbide should be taken into account as so that to determine if material makeup has any effect on the results.

REFERENCES

[1] P. K. Steimer, "Power electronics, a key technology for future more electrical energy systems," *2009 IEEE Energy Convers. Congr. Expo. ECCE 2009*, pp. 1161–1165, 2009.

[2] M. Elbuluk and N. R. N. Idris, "The role power electronics in future energy systems and green industrialization," *PECon 2008 - 2008 IEEE 2nd Int. Power Energy Conf.*, no. PECon 08, pp. 1–6, 2008.

[3] D. Gielen, F. Boshell, D. Saygin, M. D. Bazilian, N. Wagner, and R. Gorini, "The role of renewable energy in the global energy transformation," *Energy Strateg. Rev.*, vol. 24, no. January, pp. 38–50, 2019.

[4] S. M. Shinde, K. D. Patil, S. S. Khairnar, and W. Z. Gandhare, "The role of power electronics in renewable energy systems research and development," *2009 2nd Int. Conf. Emerg. Trends Eng. Technol. ICETET 2009*, pp. 726–730, 2009.

[5] C. Busca *et al.*, "An overview of the reliability prediction related aspects of high power IGBTs in wind power applications," *Microelectron. Reliab.*, vol. 51, no. 9–11, pp. 1903–1907, 2011.

[6] B. K. Bose, L. Fellow, and C. Science, "Energy Scenario and Impact of Power Electronics," *IEEE Ind. Electron. Mag.*, vol. 1, no. March, pp. 6–17, 2010.

[7] M. Toyota, Z. Long Liang, Y. Akita, H. Miyata, S. Kato, and T. Kurosu, "Application of power electronics technology to energy efficiency and CO2 reduction," *Hitachi Rev.*, vol. 59, no. 4, pp. 141–148, 2010.

[8] A. Ledenev, "(12) Patent Application Publication (10) Pub. No.: US 2012/0104864 A1," vol. 1, no. 19, 2012.

[9] T. Hirose and H. Matsuo, "Standalone hybrid wind-solar power generation system applying dump power control without dump load," *IEEE Trans. Ind. Electron.*, vol. 59, no. 2, pp. 988–997, 2012.

[10] O. Ellabban, H. Abu-Rub, and F. Blaabjerg, "Renewable energy resources: Current status, future prospects and their enabling technology," *Renew. Sustain. Energy Rev.*, vol. 39, pp. 748–764, 2014.

[11] O. Edenhofer *et al.*, *IPCC, 2011: Summary for Policymakers. In: IPCC Special Report on Renewable Energy Sources and Climate Change Mitigation*. 2011.

[12] A. Middendorf, S. Benecke, N. F. Nissen, O. Wittler, and K. D. Lang, "Establishing EcoReliability of electronic devices in manufacturing environments," *Procedia CIRP*, vol. 26, pp. 436–442, 2015.

[13] M. Florkowski, "Switched-Capacitor Power Electronics Circuits," *IEEE Electr. Insul. Mag.*, vol. 36, no. 2, pp. 53–54, 2020.

[14] J. M. Carrasco *et al.*, "Power-electronic systems for the grid integration of renewable energy sources: A survey," *IEEE Trans. Ind. Electron.*, vol. 53, no. 4, pp. 1002–1016, 2006.

[15] T. J. Karkkainen *et al.*, “Acoustic emission in power semiconductor modules-First observations,” *IEEE Trans. Power Electron.*, vol. 29, no. 11, pp. 6081–6086, 2014.

[16] A. Albarbar and C. Batunlu, *Thermal Analysis of Power Electronic Devices Used in Renewable Energy Systems*. 2017.

[17] H. Wu, C. Ye, Y. Zhang, J. Nie, Y. Kuang, and Z. Li, “Remaining Useful Life Prediction of an IGBT Module in Electric Vehicles Statistical Analysis,” *Symmetry (Basel).*, vol. 12, no. 8, p. 1325, 2020.

[18] R. Wu, F. Blaabjerg, H. Wang, M. Liserre, and F. Iannuzzo, “Catastrophic failure and fault-tolerant design of IGBT power electronic converters - An overview,” *IECON Proc. (Industrial Electron. Conf.*, pp. 507–513, 2013.

[19] C. Y. Yin, H. Lu, M. Musallam, C. Bailey, and C. M. Johnson, “A prognostic assessment method for power electronics modules,” *Proc. - 2008 2nd Electron. Syst. Technol. Conf. ESTC*, pp. 1353–1358, 2008.

[20] U. M. Choi, F. Blaabjerg, and K. B. Lee, “Study and handling methods of power IGBT Module failures in power electronic converter systems,” *IEEE Trans. Power Electron.*, vol. 30, no. 5, pp. 2517–2533, 2015.

[21] B. Ji, V. Pickert, W. Cao, and B. Zahawi, “In situ diagnostics and prognostics of wire bonding faults in IGBT modules for electric vehicle drives,” *IEEE Trans. Power Electron.*, vol. 28, no. 12, pp. 5568–5577, 2013.

[22] M. Ciappa, “Selected failure mechanisms of modern power modules,” *Microelectron. Reliab.*, vol. 42, no. 4–5, pp. 653–667, 2002.

[23] N. Jiang *et al.*, “Reliability issues of lead-free solder joints in electronic devices,” *Sci. Technol. Adv. Mater.*, vol. 20, no. 1, pp. 876–901, 2019.

[24] M. J. Barnes *et al.*, “Analysis of High-Power IGBT Short Circuit Failures,” *IEEE Trans. Plasma Sci.*, vol. 33, no. 4, pp. 1252–1261, 2005.

[25] Y. Hassan Ali, R. Abd Rahman, and R. I. Raja Hamzah, “Acoustic emission signal analysis and artificial intelligence techniques in machine condition monitoring and fault diagnosis: A review,” *J. Teknol. (Sciences Eng.*, vol. 69, no. 2, pp. 121–126, 2014.

[26] P. Ghimire, A. R. De Vega, S. Beczkowski, B. Rannestad, S. Munk-Nielsen, and P. Thogersen, “Improving power converter reliability: Online monitoring of high-power IGBT modules,” *IEEE Ind. Electron. Mag.*, vol. 8, no. 3, pp. 40–50, 2014.

[27] . A. P., “Acoustic Emission Condition Monitoring: an Application for Wind Turbine Fault Detection,” *Int. J. Res. Eng. Technol.*, vol. 02, no. 06, pp. 907–918, 2013.

[28] H. Oh, B. Han, P. McCluskey, C. Han, and B. D. Youn, “Physics-of-failure, condition monitoring, and prognostics of insulated gate bipolar transistor modules: A review,” *IEEE Trans. Power Electron.*, vol. 30, no. 5, pp. 2413–2426, 2015.

[29] U. M. Choi *et al.*, “Power cycling test and failure analysis of molded Intelligent Power IGBT Module under different temperature swing durations,” *Microelectron. Reliab.*, vol. 64, pp. 403–408, 2016.

[30] A. Saeed, “Online Condition Monitoring System for Wind Turbine Case Study,” no. October, p. 79, 2008.

[31] F. Blaabjerg, K. Ma, and Y. Yang, "Power electronics for renewable energy systems – Status and trends," *CIPS 2014 - 8th Int. Conf. Integr. Power Electron. Syst. Proc.*, pp. 25–27, 2014.

[32] W. Yang, *Condition monitoring of offshore wind turbines*. Elsevier Ltd, 2016.

[33] S. Yang, D. Xiang, A. Bryant, P. Mawby, L. Ran, and P. Tavner, "Condition monitoring for device reliability in power electronic converters: A review," *IEEE Trans. Power Electron.*, vol. 25, no. 11, pp. 2734–2752, 2010.

[34] R. Moeini, "Early failure detection of insulated-gate bipolar transistor semiconductor devices for the power converters of wind turbines," 2020.

[35] D. Mba and R. B. K. N. Rao, "Development of acoustic emission technology for condition monitoring and diagnosis of rotating machines: Bearings, pumps, gearboxes, engines, and rotating structures," *Shock Vib. Dig.*, vol. 38, no. 2, pp. 3–16, 2006.

[36] S. Lazić *et al.*, "Dynamically tuned non-classical light emission from atomic defects in hexagonal boron nitride," *Commun. Phys.*, vol. 2, no. 1, pp. 1–8, 2019.

[37] S. Müller, C. Drechsler, U. Heinkel, and C. Herold, "Acoustic emission for state-of-health determination in power modules," *13th Int. Multi-Conference Syst. Signals Devices, SSD 2016*, pp. 468–471, 2016.

[38] J. K. Ferrell and E. P. Stahel, *Heat transfer*, vol. 58, no. 12. 1966.

[39] C. Qian *et al.*, "Thermal Management on IGBT Power Electronic Devices and Modules," *IEEE Access*, vol. 6, pp. 12868–12884, 2018.

[40] A. Hamidi, N. Beck, K. Thomas, and E. Herr, "Reliability and lifetime evaluation of different wire bonding technologies for high power IGBT modules," *Microelectron. Reliab.*, vol. 39, no. 6–7, pp. 1153–1158, 1999.

[41] F. A. Stam and E. Davitt, "Effects of thermomechanical cycling on lead and lead-free (SnPb and SnAgCu) surface mount solder joints," *Microelectron. Reliab.*, vol. 41, no. 11, pp. 1815–1822, 2001.

[42] Fuji Electric, "Chapter 11 Reliability of power module," in *6th-Generation V-Series IGBT Module Application Manual*, pp. 1–11.

[43] G. Sharon and G. Caswell, "Temperature cycling and fatigue in electronics," *Adv. Microelectron.*, vol. 42, no. 5, pp. 18–24, 2015.

[44] H. Chen, B. Ji, V. Pickert, and W. Cao, "Real-time temperature estimation for power MOSFETs considering thermal aging effects," *IEEE Trans. Device Mater. Reliab.*, vol. 14, no. 1, pp. 220–228, 2014.

[45] B. Hu *et al.*, "Failure and Reliability Analysis of a SiC Power Module Based on Stress Comparison to a Si Device," *IEEE Trans. Device Mater. Reliab.*, vol. 17, no. 4, pp. 727–737, 2017.

[46] R. Wu *et al.*, "A Temperature-Dependent Thermal Model of IGBT Modules Suitable for Circuit-Level Simulations," *IEEE Trans. Ind. Appl.*, vol. 52, no. 4, pp. 3306–3314, 2016.

[47] M. März and P. Nance, "Thermal Modeling of Power Electronic Systems," *Infineon*

Technol. AG Munich, pp. 1–20, 2000.

[48] S. De Filippis, “Modeling, Simulation and Validation of the Electro-Thermal Interaction in Power Mosfets,” pp. 1–169, 2012.

[49] O. Schilling, M. Schäfer, K. Mainka, M. Thoben, and F. Sauerland, “Power cycling testing and FE modelling focussed on Al wire bond fatigue in high power IGBT modules,” *Microelectron. Reliab.*, vol. 52, no. 9–10, pp. 2347–2352, 2012.

[50] I. F. Kovačević-Badstuebner, J. W. Kolar, and U. Schilling, “Modelling for the lifetime prediction of power semiconductor modules,” *Reliab. Power Electron. Convert. Syst.*, pp. 103–140, 2016.

[51] C. Ming, H. An, W. Bo, and T. Yong, “Test of IGBT junction-case steady state thermal resistance and experimental analysis,” *Proc. - 2010 Int. Conf. Intell. Syst. Des. Eng. Appl. ISDEA 2010*, vol. 2, pp. 557–560, 2010.

[52] Y. Bao and Q. Jiang, “Summary of Life Prediction and Failure Analysis of IGBT Modules Based on Accelerated Aging Test,” *2019 22nd Int. Conf. Electr. Mach. Syst. ICEMS 2019*, 2019.

[53] C. Tang, “Thermal modelling of a mutlichip IGBT power module Keywords The investigated IGBT module and conditions,” *2019 21st Eur. Conf. Power Electron. Appl. (EPE ’19 ECCE Eur.*, pp. 1–8, 2020.

[54] T. Azoui, S. Verde, J. B. Sauveplane, and P. Tounsi, “3D Electro-Thermal Study for Reliability of Automotive Power Vertical MOSFET Using COMSOL Multiphysics,” pp. 3–6, 2009.

[55] M. Ahsan, S. T. Hon, C. Batunlu, and A. Albarbar, “Reliability Assessment of IGBT through Modelling and Experimental Testing,” *IEEE Access*, vol. 8, pp. 39561–39573, 2020.

[56] Z. Khatir and S. Lefebvre, “Boundary element analysis of thermal fatigue effects on high power IGBT modules,” *Microelectron. Reliab.*, vol. 44, no. 6, pp. 929–938, 2004.

[57] A. S. Bahman, K. Ma, and F. Blaabjerg, “FEM Thermal Modeling and Improvement for High Power IGBT Modules Used in Wind Turbine Systems,” *Proc. Int. Conf. Wind energy Grid-Adaptive Technol. WEGAT 2014*, pp. 1-7 BT-Proceedings of the International Conferen, 2014.

[58] P. A. Owusu and S. Asumadu-Sarkodie, “A review of renewable energy sources, sustainability issues and climate change mitigation,” *Cogent Eng.*, vol. 3, no. 1, pp. 1–14, 2016.

[59] F. Hassanzadeh, H. Sangrody, A. Hajizadeh, and S. Akhlaghi, “Back-to-back converter control of grid-connected wind turbine to mitigate voltage drop caused by faults,” *2017 North Am. Power Symp. NAPS 2017*, 2017.

[60] T. J. Karkkainen, J. P. Talvitie, M. Kuisma, P. Silventoinen, and E. Mengotti, “Measurement challenges in acoustic emission research of semiconductors,” *2015 17th Eur. Conf. Power Electron. Appl. EPE-ECCE Eur. 2015*, pp. 1–6, 2015.

[61] T. Kärkkäinen, *Observations of Acoustic Emission in Power Semiconductors*. 2015.

[62] M. Ciappa and A. Castellazzi, “Reliability of high-power IGBT modules for traction

applications," *Annu. Proc. - Reliab. Phys.*, no. May, pp. 480–485, 2007.

[63] T. J. Karkkainen, J. P. Talvitie, M. Kuisma, P. Silventoinen, and E. Mengotti, "Acoustic emission caused by the failure of a power transistor," *Conf. Proc. - IEEE Appl. Power Electron. Conf. Expo. - APEC*, vol. 2015-May, no. May, pp. 2481–2484, 2015.

[64] T. J. Kärkkäinen, J. P. Talvitie, O. Ikonen, M. Kuisma, P. Silventoinen, and E. Mengotti, "Sounds from semiconductors - Acoustic emission experiment with a power module," *2014 16th Eur. Conf. Power Electron. Appl. EPE-ECCE Eur. 2014*, pp. 1–6, 2014.

[65] Comsol Ab, "Acoustics Module," *Interfaces (Providence).*, p. 214, 2010.

[66] L. E. Kinsler, A. R. Frey, and W. G. Mayer, " Fundamentals of Acoustics ," *Phys. Today*, vol. 16, no. 8, pp. 56–57, 1963.

[67] H. Jensen, "How to Model Thermoviscous Acoustics in COMSOL Multiphysics Considerations for Modeling Thermoviscous Acoustics." 2014.

[68] W. Na, *Frequency Domain Linearized Navier-Stokes Equations Methodology for Aero-Acoustic and Thermoacoustic Simulations*. 2015.

[69] "The Acoustics Module User's Guide," pp. 1–542, 2014.

[70] D. D. E. La and C. Universite, "A Systematic Approach to Reliability Assessment of DC-DC Power Electronic Converters," 2016.

[71] R. Stadler and A. Maurer, "Methods for durability testing and lifetime estimation of thermal interface materials in batteries," *Batteries*, vol. 5, no. 1, pp. 1–11, 2019.

[72] A. Fatemi and L. Yang, "Cumulative fatigue damage and life prediction theories: A survey of the state of the art for homogeneous materials," *Int. J. Fatigue*, vol. 20, no. 1, pp. 9–34, 1998.

APPENDICES

Table A.1 Sound pressure level from 10 kHz to 100 kHz at 75w

(Steps of 10000 each)

Frequency (Hz)	Sound pressure level (dB), Point: (4.95, 0.005, -5)
10000	89.198
20000	103.99
30000	91.611
40000	88.059
50000	117.2
60000	96.71
70000	93.636
80000	67.591
90000	106.49
1.00E+05	95.199

Table A.2 Sound pressure level from 10 kHz to 100 kHz at 75w

(Steps of 5000 each)

Frequency (Hz)	Sound pressure level (dB), Point: (4.95, 0.005, -5)
10000	89.198
15000	103.65
20000	103.99
25000	98.682
30000	91.611
35000	79.841
40000	88.059
45000	107.91
50000	117.2
55000	122.47
60000	96.71
65000	102.91
70000	93.636
75000	88.529
80000	67.591
85000	89.943
90000	106.49
95000	86.62
1.00E+05	95.199

Table A.3 Sound pressure level from 10Hz to 9010HZ at 75w

(Steps of 1000 each)

Frequency (Hz)	Sound pressure level (dB), Point: (4.95, 0.005, -5)
10	86.668
1010	91.047
2010	89.939
3010	99.254
4010	97.273
5010	105
6010	98.622
7010	107.62
8010	109.72
9010	102.18

Table A.4 Sound pressure level from 10kHz to 90kHZ at 75w

(Steps of 20000 each)

Frequency (Hz)	Sound pressure level (dB), Point: (4.95, 0.005, -5)
10000	89.346
30000	92.171
50000	117.13
70000	94.373
90000	106.51

Table A.5 Sound pressure level from 1 kHz to 9 kHz at 75w

(Steps of 2000 each)

Frequency (Hz)	Sound pressure level (dB), Point: (4.95, 0.005, -5)
1000	90.935
3000	98.515
5000	106.42
7000	105.48
9000	131.24

Table A.6 Sound pressure level from 1 kHz to 10 kHz at 75w

(Steps of 1000 each)

Frequency (Hz)	Sound pressure level (dB), Point: (4.95, 0.005, -5)
1000	90.935
2000	90.285
3000	98.515
4000	97.266
5000	106.42
6000	100.93
7000	105.48
8000	108.97
9000	131.24
10000	89.346

IGBT Model in Air Showing the Different Probe Points

.

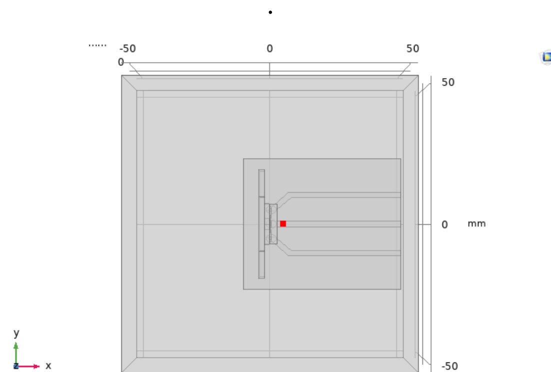

(a) Domain probe 1 :(4.95, 0.005, -5).

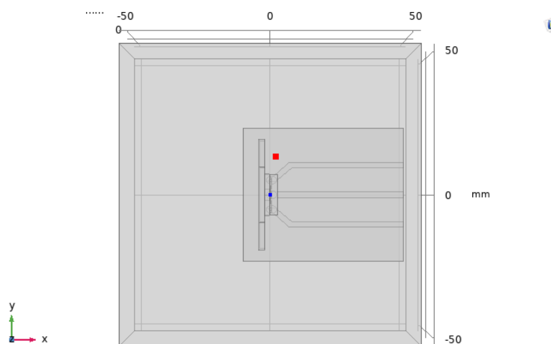

(b) Domain probe 2 :(1.95, 14, 0).

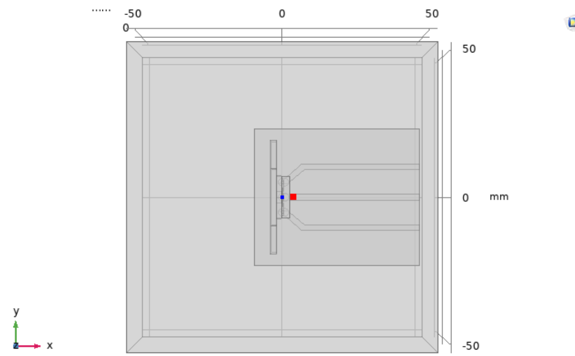

(c) Domain probe 3 :(3.95, 0.005, -6).

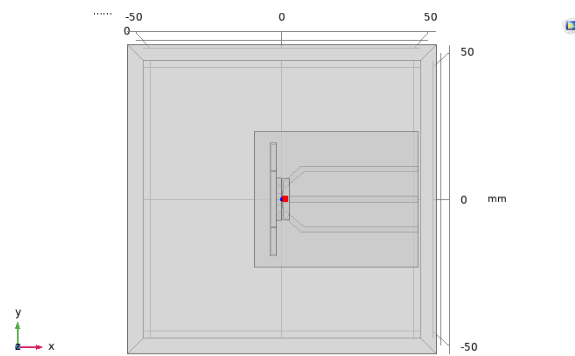

(d) Domain probe 4 :(0.95, 0.006, -4).

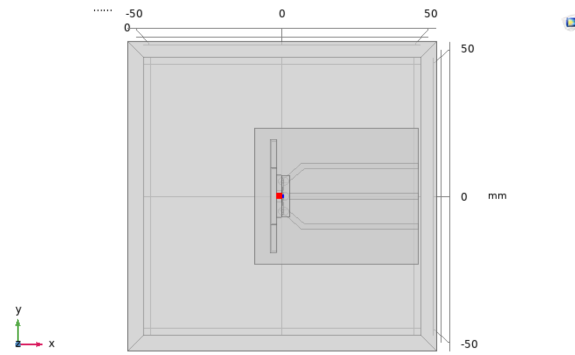

Domain probe 5:(-0.95, 0.005, and -5).

Figure A.1 IGBT Model in Air Showing the Different Probe Points

Table A.7 Sound Pressure Levels at Different Strategic Positions of the Chip

freq (Hz)	Sound pressure level (dB), Point: (4.95, 0.005, -5)	Sound pressure level (dB), Point: (1.95, 14, 0)	Sound pressure level (dB), Point: (3.95, 0.005, -6)	Sound pressure level (dB), Point: (0.95, 0.006, -4)	Sound pressure level (dB), Point: (-0.95, 0.005, -5)
30000	92.171	104.46	94.108	114.54	117.27
40000	87.666	103.67	86.123	105.52	111.56
50000	117.13	114.55	123.42	125.97	135.14
60000	96.336	105.15	104.78	105.5	110.93
freq (Hz)	Sound pressure level (dB), Point: (4.95, 0.005, -5)	Sound pressure level (dB), Point: (1.95, 14, 0)	Sound pressure level (dB), Point: (3.95, 0.005, -6)	Sound pressure level (dB), Point: (0.95, 0.006, -4)	Sound pressure level (dB), Point: (-0.95, 0.005, -5)
3000	98.515	93.019	98.276	95.483	75.711
4000	97.266	94.661	97.257	96.043	92.63
5000	106.42	105.82	106.56	106.67	106.72
6000	100.93	100.84	101.05	101.45	101.42
freq (Hz)	Sound pressure level (dB), Point: (4.95, 0.005, -5)	Sound pressure level (dB), Point: (1.95, 14, 0)	Sound pressure level (dB), Point: (3.95, 0.005, -6)	Sound pressure level (dB), Point: (0.95, 0.006, -4)	Sound pressure level (dB), Point: (-0.95, 0.005, -5)
300	87.02	86.31	86.975	86.553	85.472
400	87.271	86.577	87.227	86.813	85.75
500	87.603	86.931	87.561	87.157	86.118
600	88.025	87.38	87.984	87.593	86.585
freq (Hz)	Sound pressure level (dB), Point: (4.95, 0.005, -5)	Sound pressure level (dB), Point: (1.95, 14,	Sound pressure level (dB), Point: (3.95, 0.005, -6)	Sound pressure level (dB), Point: (0.95, 0.006, -4)	Sound pressure level (dB), Point: (-0.95, 0.005, -5)

		0)			
30	86.708	85.988	86.67	86.223	85.121
40	86.719	85.988	86.681	86.235	85.134
50	86.725	85.99	86.686	86.243	85.141
60	86.73	85.993	86.69	86.248	85.147

Graphs representing data from Table 2 above.

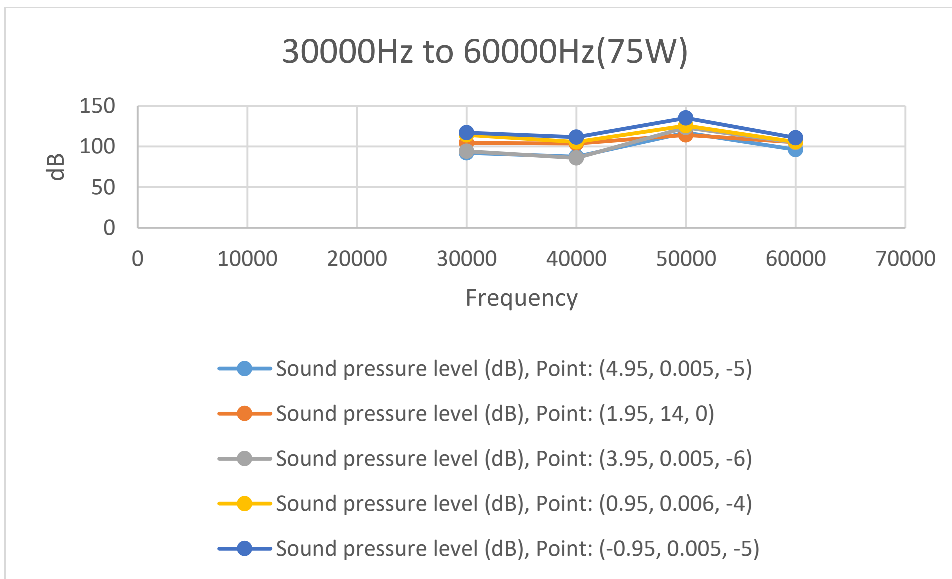

Figure A.2 30000Hz to 60000Hz (75W)

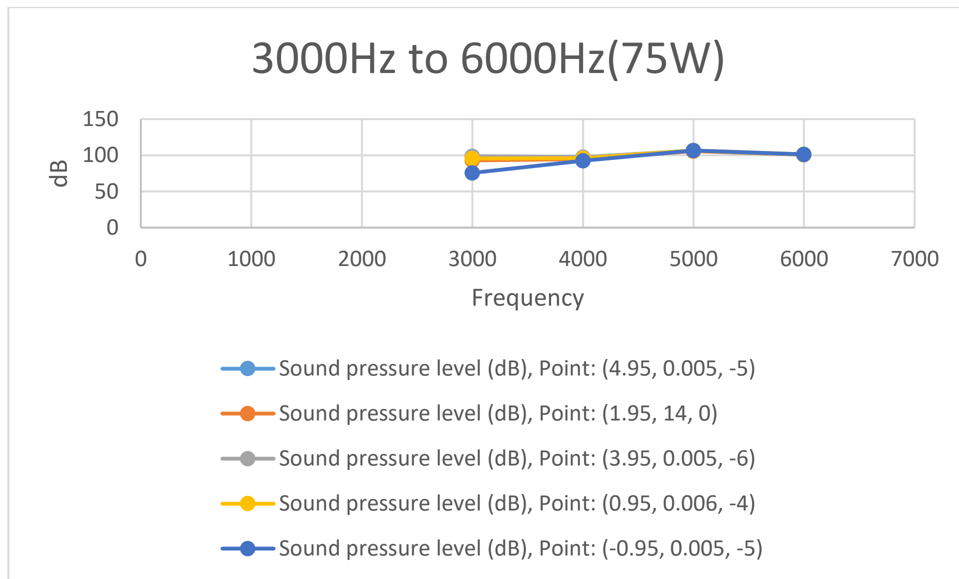

Figure A.3 3000Hz to 6000Hz (75W).

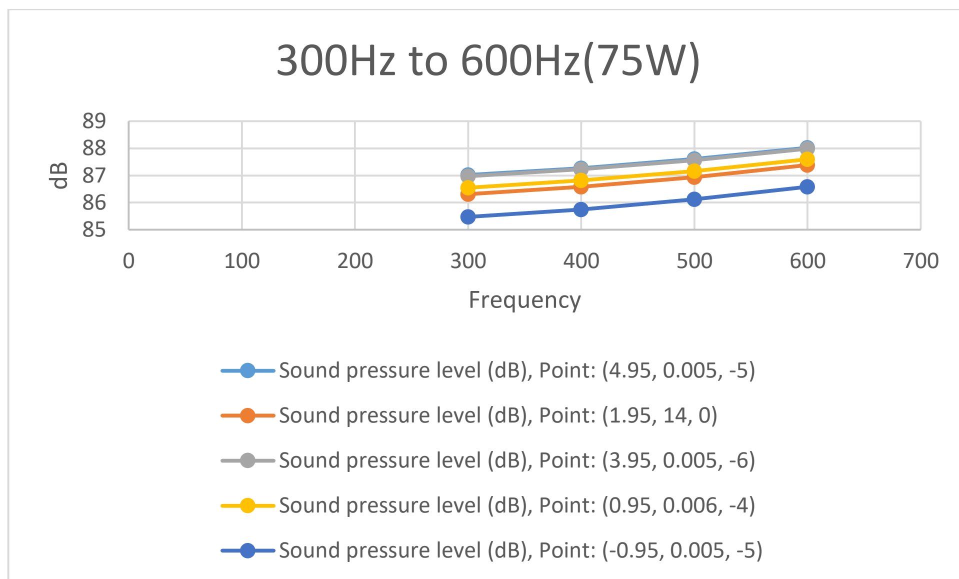

Figure A.4 300Hz to 600Hz (75W).

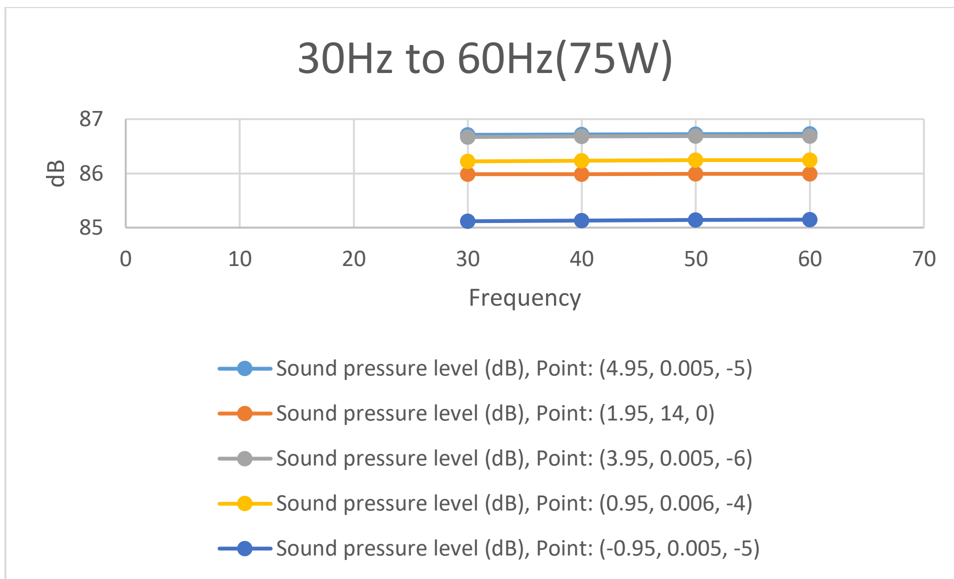

Figure A.5 30Hz to 60Hz (75W).

Table A.8 Heat (W) against Temperature (degC).

Heat(W)	Temperature(degC)
0.75	36
7.5	133
75	1144

Table A.9 Heat (W) against Sound Pressure Level (dB).

Heat(W)	Sound pressure level (dB
0.75	93.985
7.5	93.996
75	94.108
750	95.289
7500	104.2

Table A.10 Temperature (degC) against Sound Pressure Level (dB).

Temperature(degC)	Sound pressure level (dB)
36	93.985
133	93.996
1144	94.108

Table A.11 Sound Pressure Level against Temperature (deg C).

Sound pressure level (dB)	Temperature(degC)
93.985	36
93.996	133
94.108	1144

Table A.12 Temperature (degC) against Sound Pressure Level (dB).

Temperature(degC)	Sound pressure level (dB)
36	93.985
133	93.996
1144	94.108

Table A.13 Relation between Number of Cycles Mean Temperature and Change in Temperature

Number of cycles	Mean Temp(degC)	Change in temp (ΔT)
4	42.83	3.93
2	40.22	0.95
2	35.83	2.54
2	30	1.69
2	41.13	3.99
2	49.48	9.12
3	38.75	4.58
2	46.35	8.29

Table A.14 Determining the value of Nf

Tmean (k)	ΔT	Number of cycles		N_f
298.0005	0.007	1	1.91448E-22	1.91448E-22

303.0915	0.019	1	4.79656E-20	4.79656E-20
320.4765	0.485	1	2.80615E-12	2.80615E-12
300.9335	0.595	1	1.15598E-12	1.15598E-12
298.394	0.78	1	3.42877E-12	3.42877E-12
299.71	1.852	1	2.97217E-10	2.97217E-10
305.5635	1.951	1	7.04123E-10	7.04123E-10
304.607	2.274	1	1.3749E-09	1.3749E-09
321.681	2.65	1	1.52557E-08	1.52557E-08
326.2675	2.965	1	4.03748E-08	4.03748E-08
310.5135	3.077	1	1.12315E-08	1.12315E-08
330.936	3.278	1	1.00213E-07	1.00213E-07
308.1935	3.309	1	1.28559E-08	1.28559E-08
312.4325	3.331	1	2.01187E-08	2.01187E-08
312.576	4.01	1	5.15774E-08	5.15774E-08
318.3475	4.017	1	8.98539E-08	8.98539E-08
307.796	4.104	1	3.6267E-08	3.6267E-08
314.239	4.374	1	9.3411E-08	9.3411E-08
319.862	4.434	1	1.69377E-07	1.69377E-07
324.4255	4.693	1	3.40444E-07	3.40444E-07
321.4675	5.009	1	3.61003E-07	3.61003E-07
313.553	5.572	1	2.93478E-07	2.93478E-07
309.6255	5.619	1	2.09078E-07	2.09078E-07
326.206	6.182	1	1.58223E-06	1.58223E-06
306.6255	6.311	1	2.77476E-07	2.77476E-07
319.9395	6.351	1	1.02846E-06	1.02846E-06
324.2345	7.031	1	2.52609E-06	2.52609E-06
321.2085	7.067	1	1.97092E-06	1.97092E-06
316.5695	7.313	1	1.52169E-06	1.52169E-06
322.753	8.038	1	4.31703E-06	4.31703E-06
324.2745	8.081	1	5.08447E-06	5.08447E-06
316.012	8.338	1	2.78201E-06	2.78201E-06
321.4815	9.435	1	8.57077E-06	8.57077E-06
313.637	10.652	1	7.55389E-06	7.55389E-06
319.394	13.61	1	4.42004E-05	4.42004E-05
313.2263	0.95	2	4.09759E-11	8.19519E-11
303	1.69	2	2.64557E-10	5.29114E-10
308.831	2.54	2	3.64912E-09	7.29825E-09
316.545	3.99	2	7.34029E-08	1.46806E-07
313.79	9.12	2	3.52654E-06	7.05308E-06
319.3	8.29	2	3.67398E-06	7.34796E-06
311.75	4.56	3	9.05488E-08	2.71646E-07
315.83	3.93	4	6.36139E-08	2.54456E-07

Table A.15 Relationship between Nf Mean temperature and Change in temperature

Nf	Mean Temp(K)	Change in temp (DT)
5.29E-10	303	1.69
7.3E-09	308.831	2.54
3.56E-06	319.8985	8.147
1.47E-07	316.545	3.99
3.8E-06	318.7935	8.425
7.05E-06	313.79	9.12
7.35E-06	319.3	8.29
2.72E-07	311.75	4.56
2.54E-07	315.83	3.93